

Pion form factor in QCD: From nonlocal condensates to NLO analytic perturbation theory

A. P. Bakulev*

Bogoliubov Laboratory of Theoretical Physics, JINR, 141980 Dubna, Russia

K. Passek-Kumerički†

*Theoretical Physics Division, Rudjer-Bošković Institute,
P.O. Box 180, HR-10002 Zagreb, Croatia*

W. Schroers‡

*Center for Theoretical Physics, Laboratory for Nuclear Science and Department of Physics,
Massachusetts Institute of Technology, Cambridge Massachusetts 02139*

N. G. Stefanis§

*Institut für Theoretische Physik II,
Ruhr-Universität Bochum, D-44780 Bochum, Germany*

Abstract

We present an investigation of the pion's electromagnetic form factor $F_\pi(Q^2)$ in the spacelike region utilizing two new ingredients: (i) a double-humped, endpoint-suppressed pion distribution amplitude derived before via QCD sum rules with nonlocal condensates—found to comply at the 1σ level with the CLEO data on the $\pi\gamma$ transition—and (ii) analytic perturbation theory at the level of parton amplitudes for hadronic reactions. The computation of $F_\pi(Q^2)$ within this approach is performed at NLO of QCD perturbation theory (standard and analytic), including the evolution of the pion distribution amplitude at the same order. We consider the NLO corrections to the form factor in the $\overline{\text{MS}}$ scheme with various renormalization scale settings and also in the α_V -scheme. We find that using standard perturbation theory, the size of the NLO corrections is quite sensitive to the adopted renormalization scheme and scale setting. The main results of our analysis are the following: (i) Replacing the QCD coupling and its powers by their analytic images, both dependencies are diminished and the predictions for the pion form factor are quasi scheme and scale-setting independent. (ii) The magnitude of the factorized pion form factor, calculated with the aforementioned pion distribution amplitude, is only slightly larger than the result obtained with the asymptotic one in all considered schemes. (iii) Including the soft pion form factor via local duality and ensuring the Ward identity at $Q^2 = 0$, we present predictions that are in remarkably good agreement with the existing experimental data both in trend and magnitude.

PACS numbers: 11.10.Hi, 12.38.Bx, 12.38.Cy, 13.40.Gp

*Electronic address: bakulev@thsun1.jinr.ru

†Electronic address: passek@thphys.irb.hr

‡Electronic address: wolfram.schroers@feldtheorie.de

§Electronic address: stefanis@tp2.ruhr-uni-bochum.de

I. INTRODUCTION

It is the purpose of this paper to review and discuss questions relating to the calculation of the electromagnetic pion form factor with an improved pion distribution amplitude (DA), derived from QCD sum rules with nonlocal condensates [1], and to use QCD Analytic Perturbation Theory (APT) [2, 3, 4, 5, 6] beyond the leading order (LO). Before going into the details of this framework, let us expose, in general terms, what these two ingredients mean for the analysis and also make some introductory remarks.

Hadronic form factors are typical examples of hard-scattering processes within QCD [7, 8, 9, 10, 11, 12] and clearly the first level of knowledge necessary to understand the structure of *intact* hadrons in terms of quarks and gluons. Such processes have been much explored both because of their physical relevance, as being accessible to experiments, and because they allow to assess nonperturbative features of QCD (for reviews, see, for instance, [13, 14, 15, 16, 17]). In the following, the discussion is centered around the pion’s electromagnetic form factor. At a more theoretical level, “hard” means that at least some part of the process amplitude, recast in terms of quarks collinear to hadrons (in an appropriate Lorentz frame), should become amenable to perturbation theory via factorization theorems on account of the hard-momentum scale of the process, say, Q^2 , that should suppress factorized infrared (IR) subprocesses, thus ensuring short-distance dominance. Under these circumstances one can safely evaluate logarithmic scaling violations by means of perturbative QCD (pQCD) and the renormalization-group equation. When no hard momenta flow on the side of the initial (incoming) or the final (outgoing) hadron, factorization fails and a renormalization-group analysis cannot be made, so that in order to calculate the non-factorizable part of the pion form factor, one has to resort to phenomenological models (prime examples of which are [18, 19, 20, 21]), or employ theoretical concepts like the (local) quark-hadron duality [22] and their descendants [23, 24, 25].

Despite dedicated efforts in the last two decades, exclusive processes have failed to deliver a complete quantitative understanding within QCD for a variety of reasons, among others:

- Limited knowledge of higher-order perturbative and power-law behaved (e.g., higher-twist) corrections to the amplitudes.
- Presence of singularities (of endpoint, mass, soft, collinear, or pinch origin) that may spoil factorization in some kinematic regions.
- Insignificant knowledge of hadron distribution amplitudes owing to the lack of a reliable non-perturbative approach.
- Non-factorizing contributions that are not calculable within pQCD and hence introduce a strong model dependence.

While it may still be not possible to clarify all these theoretical issues conclusively, we believe that significant progress has quite recently been achieved in understanding the pion structure both from the theoretical side—perturbatively [26, 27, 28, 29, 30] and nonperturbatively [1, 31, 32, 33, 34]—as well as from the experimental side [35, 36, 37] and associated data-processing techniques [38, 39, 40], a progress that could bring to a cleaner comparison between data and various theoretical QCD predictions [31, 39, 40, 41, 42, 43, 44, 45, 46, 47,

48, 49].¹ Moreover, a program to compute the electromagnetic and transition form factors of mesons on the lattice has been launched by two collaborations, [51, 52] and [53], that may provide valuable insights when it is completed. This situation prompts an in-depth review and update of these issues, in an effort to consolidate previous calculations of the pion’s electromagnetic form factor and narrow down theoretical uncertainties.

We will focus our present discussion on two main issues:

- (i) How QCD perturbation theory can be safely used to make predictions in the low-momentum regime where conventional power series expansions in the QCD coupling break down and nonperturbative effects dominate. Such an extension is based on recent works on “analytization” of the running strong coupling $\alpha_s(Q^2)$ [2, 3, 6, 54, 55, 56, 57, 58] (see also [59] for a slightly different approach) and their generalization to the partonic level of hadron amplitudes, like the electromagnetic and the pion-photon transition form factor, or the Drell–Yan process, beyond the level of a single scheme scale [28, 29, 60, 61]. In contradiction to the usual assumption of singular growth of $\alpha_s(Q^2)$ in the IR domain, the QCD coupling in this scheme has an IR-fixed point, with the unphysical Landau pole being completely absent. In conventional perturbative approaches, a choice of the renormalization scale in the region of a few Λ_{QCD} , as required, for instance, by the Brodsky–Lepage–Mackenzie (BLM) scale-fixing procedure [62], would induce singularities thus prohibiting the perturbative calculation of hadronic observables. Using APT, these singularities are avoided by construction, i.e., without introducing ad hoc IR regulators, e.g., an effective gluon mass [14, 63], and therefore the validity of the perturbative expansion (in mass-independent renormalization schemes) is not jeopardized by IR-renormalon power-law ambiguities. In addition, APT provides a better stability against higher-loop corrections and a weaker renormalization-scheme dependence than standard QCD perturbative expansion—see [29] and Sec. VII d.
- (ii) How to improve the nonperturbative input by employing a pion DA which incorporates the nonperturbative features of the QCD vacuum in terms of a nonlocal quark condensate [64, 65, 66, 67, 68]. This accounts for the possibility that vacuum quarks can flow with a nonzero average virtuality λ_q^2 , in an attempt to connect dynamic properties of the pion, like its electromagnetic form factor, directly with the QCD vacuum structure (we refer to [34] for further details). Within this scheme, the pion DA (termed BMS [1] in the following) turns out to be double-humped with strongly suppressed endpoints ($x = 0, 1$), the latter feature being related to the nonlocality parameter λ_q^2 . It has been advocated, for example, in [28, 29] (see also [16, 69]), that a suppression of the endpoint region (which is essentially nonperturbative) as strong as possible is a prerequisite for the self-consistent application of QCD perturbation theory within a factorization scheme.

In a recent series of papers [1, 39, 40], two of us together with S. V. Mikhailov have conducted an analysis of the CLEO data [35] on the pion-photon transition using attributes from QCD light-cone sum rules [31, 38], NLO Efremov–Radyushkin–Brodsky–Lepage (ERBL) [9, 10, 11, 12] evolution [70, 71], and detailed estimates of uncertainties owing to higher-twist contributions and NNLO perturbative corrections [30]. These works confirmed the

¹ For theoretical predictions on $F_\pi(Q^2)$ in the timelike region, see, for instance [25, 50].

gross features of the previous Schmedding–Yakovlev (SY) analysis [38]; notably, both the Chernyak–Zhitnitsky (CZ) [13] pion DA as well as the asymptotic one are incompatible with the CLEO data [35] at the 4σ - and 3σ -level, respectively, whereas the aforementioned BMS pion DA, which incorporates the vacuum nonlocality, is within the 1σ error ellipse. Moreover, this approach revealed the possibility of using the CLEO experimental data to estimate the value of the QCD vacuum correlation length λ_q^{-1} . Indeed, it turns out that the extracted value $\lambda_q^2 \simeq 0.4 \text{ GeV}^2$ is consistent with those obtained before using QCD sum rules [72, 73, 74] and also with numerical simulations on the lattice [75, 76]. In addition, it was shown [40] that the value of the inverse moment $\langle x^{-1} \rangle_\pi(\mu^2) = \int_0^1 \varphi_\pi(x; \mu^2) x^{-1} dx$ of the pion DA, calculated by means of an *independent* QCD sum rule, is compatible with that extracted from the CLEO data. These findings give us confidence to use the BMS pion DA (including also the range of its intrinsic theoretical uncertainties) in order to derive predictions for the electromagnetic pion form factor within the factorization scheme of QCD at NLO, presenting also results which include the non-factorizing soft contribution [23, 25] to compare with available experimental data.

The structure of the paper is as follows. In Sec. II we shall recall the QCD factorization of the pion’s electromagnetic form factor. Sec. III deals with the basics of the pion distribution amplitude and its derivation from QCD sum rules with nonlocal condensates. The perturbative results for the pion form factor at NLO order, on the basis of the results given in [26], are summarized in Sec. IV, whereas issues related to the setting of the renormalization scheme and scale are discussed in Sec. V. The important topic of the non-power series expansion of the pion form factor in the context of Analytic Perturbation Theory is considered in Sec. VI. Our numerical analysis and the comparison of our results with available experimental data is presented in Sec. VII. Finally, in Sec. VIII we give a summary of the results and draw our conclusions. Important technical details of the analysis are supplied in five appendixes.

II. QCD FACTORIZATION APPLIED TO THE PION FORM FACTOR

The outstanding virtue of factorization is that a hadronic process can be dissected in such a way as to isolate a partonic part accessible to pQCD. Provided that the partonic subprocesses are free of IR-singularities, then at large momentum transfer $F_\pi(Q^2)/f_\pi^2 \sim 1/Q^2$, modulo logarithmic corrections due to renormalization. Hence, the amplitude for the electromagnetic pion form factor is short-distance dominated and can be expressed in terms of its constituent quarks collinear to the pion with the errors of this replacement being suppressed by powers of $1/Q$. Even more, one can rigorously dissect the QCD amplitude into a coefficient function, that contains the hard quark-gluon interactions, and two matrix elements corresponding to the initial and final pion states of the leading twist operator with the quantum numbers of the pion according to the Operator Product Expansion (OPE). In this way, one establishes that the coefficient function will scale asymptotically according to its dimensionality modulo anomalous dimensions controlled by the renormalization group equation.

The pion’s electromagnetic form factor is defined by the matrix element

$$\langle \pi^+(P') | J_\mu(0) | \pi^+(P) \rangle = (P + P')_\mu F_\pi(Q^2), \quad (2.1)$$

where J_μ is the electromagnetic current expressed in terms of quark fields, $(P' - P)^2 = q^2 \equiv -Q^2$ is the photon virtuality, i.e., the large momentum transfer injected into the pion, and

F_π is normalized to $F_\pi(0) = 1$. Based on the above considerations, the pion form factor can be generically written in the form [9, 10, 11, 12]

$$F_\pi(Q^2) = F_\pi^{\text{Fact}}(Q^2) + F_\pi^{\text{non-Fact}}(Q^2), \quad (2.2)$$

where $F_\pi^{\text{Fact}}(Q^2)$ is the factorized part within pQCD and $F_\pi^{\text{non-Fact}}(Q^2)$ is the non-factorizable part—usually being referred to as the “soft contribution” [23]—that contains subleading power-behaved (e.g., twist-4 and higher-twist) contributions originating from nonperturbative effects. It is important to understand that Eq. (2.2) becomes increasingly unreliable as $Q^2 \rightarrow 0$, owing to the breakdown of perturbation theory at such low momentum scales. Hence, we expect the real form factor to be different from the RHS of this equation at low Q^2 . We shall show in Sec. VII D how to remedy this problem. The leading-twist factorizable contribution can be expressed as a convolution in the form

$$F_\pi^{\text{Fact}}(Q^2; \mu_R^2) = \Phi_\pi^*(x, \mu_F^2) \otimes_x T_H(x, y, Q^2; \mu_F^2, \mu_R^2) \otimes_y \Phi_\pi(y, \mu_F^2), \quad (2.3)$$

where \otimes denotes the usual convolution symbol ($A(z) \otimes B(z) \equiv \int_0^1 dz A(z) B(z)$) over the longitudinal momentum fraction variable x (y) and μ_F represents the factorization scale at which the separation between the long- (small transverse momentum) and short-distance (large transverse momentum) dynamics takes place, with μ_R standing for the renormalization (coupling constant) scale. A graphic illustration of the factorized pion form factor in terms of Feynman diagrams is given in Fig. 1.

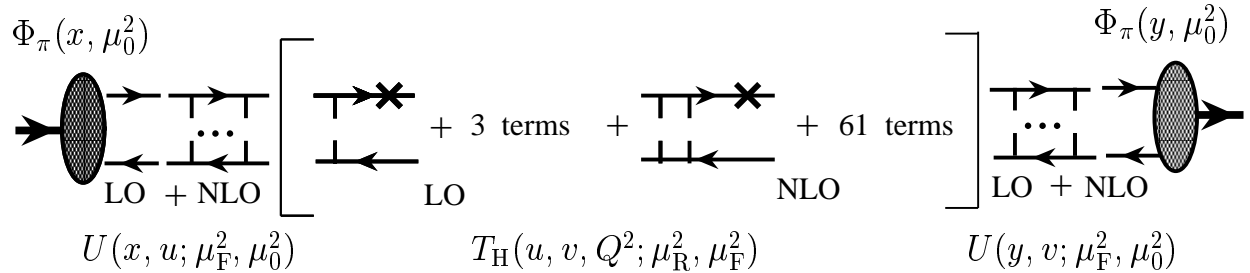


FIG. 1: Illustration of the structure of the factorized pion form factor within pQCD at NLO of the hard scattering amplitude and the evolution effect of the pion DA. Hard gluons are indicated by broken lines, whereas the external off-shell photon is denoted by a cross.

Here, $T_H(x, y, Q^2; \mu_F^2, \mu_R^2)$ is the hard-scattering amplitude, describing short-distance interactions at the parton level, i.e., it is the amplitude for a collinear valence quark-antiquark pair with total momentum P struck by a virtual photon with momentum q to end up again in a configuration of a parallel valence quark-antiquark pair with momentum $P' = P + q$ and can be calculated perturbatively in the form of an expansion in the QCD coupling, the latter to be evaluated at the reference scale of renormalization μ_R^2 :

$$T_H(x, y, Q^2; \mu_F^2, \mu_R^2) = \alpha_s(\mu_R^2) T_H^{(0)}(x, y, Q^2) + \frac{\alpha_s^2(\mu_R^2)}{4\pi} T_H^{(1)}(x, y, Q^2; \mu_F^2, \mu_R^2) + \dots \quad (2.4)$$

The explicit results for the hard-scattering amplitude in LO and NLO accuracy are supplied in Appendix A. All transverse momenta below the factorization scale that would cause

divergences associated with the propagation of partons over long distances have been absorbed into the pion DAs, which have the correct long-distance behavior, as dictated by nonperturbative QCD.

Because the QCD perturbation series expansion in the strong coupling is only asymptotic, this calculation bears an intrinsic error owing to its truncation that is of the order of the first neglected term $\sim C/Q^p$, with C and p being, in general, dependent on the particular observable in question—here the pion form factor. Lacking all-order results for the perturbative coefficients, one has to resort to fixed-order, renormalization and factorization scheme-dependent contributions to $F_\pi^{\text{Fact}}(Q^2, \mu_R^2)$ that do not exceed beyond the NLO [26]. The truncation of this series expansion at any finite order introduces a residual dependence of the corresponding fixed-order or partly resummed hard-scattering amplitude and, consequently, also of the finite-order prediction for F_π^{Fact} , on the renormalization scheme adopted and on the renormalization scale μ_R chosen. In order that the perturbative prediction comes as close as possible to the physical form factor, measured in experiments—which is exactly independent of the renormalization (or any other unphysical scheme) scale—the best perturbative expansion would be the one which minimizes the error owing to the disregarded higher-order corrections. This can be accomplished, for instance, by trading the conventional power-series perturbative expansion in favor of a non-power series expansion in terms of an analytic strong running coupling, performing the calculations in the framework of Analytic Perturbation Theory to be discussed in Sec. VI. Here it suffices to state that in this framework the QCD running coupling has an IR-fixed point and hence avoids *eo ipso* IR-renormalon ambiguities allowing to adopt a BLM scale setting procedure.

By convoluting the finite-order result for the hard-scattering amplitude, expressed in the form of Eq. (2.4), with the distribution amplitude (3.5) truncated at the same order in α_s , an additional residual dependence on the factorization scheme and the factorization scale μ_F appears. We show in Appendix B how to get rid of the factorization scale dependence at fixed order of perturbation theory (NLO) by proving that non-cancelling terms in $F_\pi^{\text{Fact}}(Q^2; \mu_R^2)$ are of order α_s^3 . For an alternative way of handling the μ_F^2 dependence, we refer the reader to [27, 77]. For practical purposes, the preferable form of the convolution equation for $F_\pi^{\text{Fact}}(Q^2)$ is given by adopting the so-called “default” choice, i.e., setting in Eqs. (2.3), (2.4) $\mu_F^2 = Q^2$. Note, however, that the same choice of scale in different schemes yields also to different results for finite-order approximants for the pion form factor [78]. Problems connected with heavy-quark mass thresholds in the β function are given below particular attention both in the hard-scattering part and in the evolution part.

Another crucial question is whether the factorizable pQCD contribution to the pion form factor is actually sufficient to describe the available experimental data, or if one has to take into account the soft part as well. It has been advocated in [18, 20, 21, 23, 25, 42, 67, 79] that at momentum-transfer values probed experimentally so far, this latter contribution, though power suppressed because it behaves like $1/Q^4$ for large Q^2 , dominates and mimics rather well the observed $1/Q^2$ behavior. To account for this effect, we will include the soft contribution [25] (discussed in Sec. VII C) into our form-factor prediction when comparing with the data, albeit the poor quality of the latter at higher Q^2 makes it impossible to draw any definite conclusions about the transition from one regime to the other. Therefore, our main purpose in this paper is to calculate the factorizable contribution as accurately as possible. The calculational ingredients will be to

- use as a nonperturbative input a set of pion DAs $\varphi_\pi(x, \mu_0^2)$, derived in [1] from QCD sum rules with nonlocal condensates, with the optimum one, termed BMS model,

standing out;

- evolve $\varphi_\pi(x, \mu_0^2)$ by employing a kernel and corresponding anomalous dimensions up to NLO [70, 71, 80] both within the standard and the analytic perturbation theory;
- employ a hard-scattering amplitude $T_H(x, y, Q^2; \mu_F^2, \mu_R^2)$ up to NLO order [26, 80, 81, 82, 83, 84, 85], using both standard power and also non-power series expansions;
- take into account the soft (non-factorizable) contribution, $F_\pi^{\text{non-Fact}}(Q^2)$, on the basis of the Local Duality (LD) approach when comparing the theoretical predictions with the experimental data.

III. PION DISTRIBUTION AMPLITUDE

A. Nonperturbative input

Turning our attention now to the pion distribution amplitude, we note that $\Phi_\pi(x, \mu_F^2)$ specifies in a process- and frame-independent way² the longitudinal-momentum xP distribution of the valence quark (and antiquark which carries a fraction $\bar{x} = 1 - x$) in the pion with momentum P . At the twist-2 level it is defined by the following universal operator matrix element (see, e.g., [13] for a review)

$$\langle 0 | \bar{d}(z) \gamma^\mu \gamma_5 \mathcal{C}(z, 0) u(0) | \pi(P) \rangle \Big|_{z^2=0} = i P^\mu \int_0^1 dx e^{ix(zP)} \Phi_\pi(x, \mu_0^2 \sim z^{-2}) ; \quad (3.1)$$

$$\int_0^1 \Phi_\pi(x, \mu_0^2) dx = f_\pi, \quad (3.2)$$

with $f_\pi = 130.7 \pm 0.4$ MeV [86] being the pion decay constant defined by

$$\langle 0 | \bar{d}(0) \gamma_\mu \gamma_5 u(0) | \pi^+(P) \rangle = i p_\mu f_\pi \quad (3.3)$$

and where

$$\mathcal{C}(0, z) = \mathcal{P} \exp \left[-i g_s \int_0^z t^a A_\mu^a(y) dy^\mu \right] \quad (3.4)$$

is the Fock–Schwinger phase factor (coined the color “connector” in [87]), path-ordered along the straight line connecting the points 0 and z , to preserve gauge invariance. The scale μ_0^2 , called the normalization scale of the pion DA, is related to the ultraviolet (UV) regularization of the quark-field operators on the light cone whose product becomes singular for $z^2 = 0$.

Although the distribution amplitude is intrinsically a nonperturbative quantity, its evolution is governed by pQCD (a detailed discussion is relegated to Appendix C) and can be expressed in the form

$$\Phi_\pi(x, \mu_F^2) = U(x, s; \mu_F^2, \mu_0^2) \otimes_s \Phi_\pi(s, \mu_0^2), \quad (3.5)$$

² Provided the same factorization scheme is used for all considered processes [16, 69].

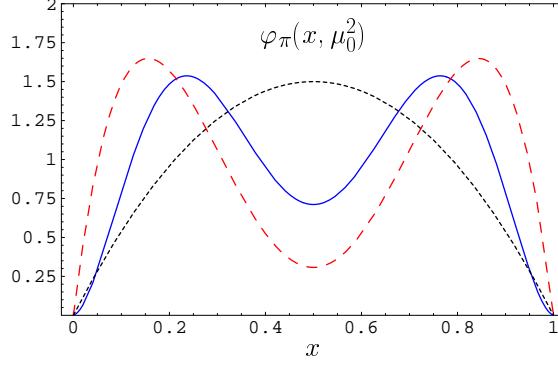


FIG. 2: Comparison of selected pion DAs denoted by obvious acronyms: φ_{as} (dotted line), φ_{CZ} (dashed line) [13], and φ_{BMS} (solid line) [1], defined by Eq. (3.8) in conjunction with (3.10). All DAs are normalized at the same scale $\mu_0^2 \approx 1 \text{ GeV}^2$.

where $\Phi_\pi(s, \mu_0^2)$ is a nonperturbative input determined at some low-energy normalization point μ_0^2 (where the local operators in Eq. (3.1) are renormalized)—which is of the order of 1 GeV^2 —while $U(x, s; \mu_F^2, \mu_0^2)$ is the operator to evolve that DA from the scale μ_0^2 to the scale μ_F^2 and is calculable in QCD perturbation theory. In the asymptotic limit, the shape of the pion DA is completely fixed by pQCD with the nonperturbative input being solely contained in f_π .

Neglecting the \mathbf{k}_\perp dependence of the hard-scattering amplitude at large Q^2 ,³ it is convenient to introduce a dimensionless pion DA, $\varphi_\pi(x)$, normalized to 1,

$$\Phi_\pi(x, \mu_0^2) = f_\pi \varphi_\pi(x, \mu_0^2) \quad (3.6)$$

that can be defined as the probability amplitude for finding two partons with longitudinal momentum fractions x and \bar{x} “smeared” over transverse momenta $\mathbf{k}_\perp^2 \leq \mu^2$, i.e.,

$$\varphi_\pi(x, \mu^2) = \int_0^{\mathbf{k}_\perp^2 \leq \mu^2} [d^2 \mathbf{k}_\perp] \psi(x, \mathbf{k}_\perp), \quad (3.7)$$

where $[d^2 \mathbf{k}_\perp]$ is an appropriate integration measure over transverse momenta [12], helicity labels have been suppressed, and a logarithmic pre-factor due to quark self-energy and photon-vertex corrections has been absorbed for the sake of simplicity into the definition of the pion wave function.

The nonperturbative input, alias the pion DA at the initial normalization scale μ_0^2 , $\varphi_\pi(x, \mu_0^2)$, will be expressed as an expansion over Gegenbauer polynomials which form an eigenfunctions decomposition, having recourse to a convenient representation which separates the x and μ^2 dependence (a detailed exposition can be found in [16]). Then, the pion DA at the initial scale μ_0^2 reads

$$\varphi_\pi(x, \mu_0^2) = 6x(1-x) \left[1 + a_2(\mu_0^2) C_2^{3/2}(2x-1) + a_4(\mu_0^2) C_4^{3/2}(2x-1) + \dots \right], \quad (3.8)$$

³ This actually means that for all initial $\mathbf{k}_{\perp i}^2 \ll Q^2$ and analogously for all final $\mathbf{l}_{\perp i}^2 \ll Q^2$, radiative corrections sense only single quark and gluon lines.

with all nonperturbative information being encapsulated in the coefficients a_n . These coefficients will be taken from a QCD sum-rules calculation employing nonlocal condensates [1, 34], and we refer the reader to these works for more details. Here we only use the results obtained there. We found at $\mu_0^2 = 1.35 \text{ GeV}^2$ and for a quark virtuality of $\lambda_q^2 = 0.4 \text{ GeV}^2$:

$$\begin{array}{lll} a_0 = 1 & a_2 = 0.19 & a_4 = -0.13 \\ a_6 = 5 \times 10^{-3} & a_8 = 4 \times 10^{-3} & a_{10} = 4 \times 10^{-3} . \end{array} \quad (3.9)$$

One appreciates that all Gegenbauer coefficients with $n > 4$ are close to zero and can therefore be neglected. Hence, to model the pion DA, it is sufficient to keep only the first two coefficients, which we display below in comparison with those for the asymptotic DA and the CZ [13] model after 2-loop evolution to the reference scale $\mu_0^2 = 1 \text{ GeV}^2$, i.e.,

$$\begin{array}{llll} \varphi_{\text{as}} : a_n = 0, n \geq 2 & & \mu_0^2 = \mu_F^2, & \\ \varphi_{\text{BMS}} : a_n = 0, n > 4 & a_2 = 0.20 & a_4 = -0.14 & \mu_0^2 = 1 \text{ GeV}^2 \\ \varphi_{\text{CZ}} : a_n = 0, n > 2 & a_2 = 0.56 & & \mu_0^2 = 1 \text{ GeV}^2 \end{array} \quad (3.10)$$

The shapes of these DAs are displayed in Fig. 2.

At this point some important remarks and observations are in order.

- The BMS pion DA, though doubly-peaked, has its endpoints $x \rightarrow 0$ and $x \rightarrow 1$ strongly suppressed due to the nonlocality parameter λ_q^2 . Hence, fears frequently expressed in the literature that double-humped pion DAs should be avoided because they may emphasize the endpoint region, where the use of perturbation theory is unjustified, are unfounded.
- The BMS pion DA approaches asymptotically φ_{as} in the endpoints from *below*, whereas φ_{CZ} approaches the asymptotic limit from *above*, which means that the endpoint behavior of the latter is dangerous until very large values of Q^2 . It is well-known [15, 16, 28] that in the endpoint region $x \rightarrow 1$ the spectator quark in the hard process, carrying the small longitudinal momentum fraction \bar{x} , can “wait” for a long time until it exchanges a soft gluon with the struck quark to fit again into the final pion wave function. As a result, a strong Sudakov suppression [88] is needed in that case in order to justify the use of perturbation theory. In contrast, the endpoint behavior of the BMS DA is not controversial because, though doubly peaked, it does not emphasize

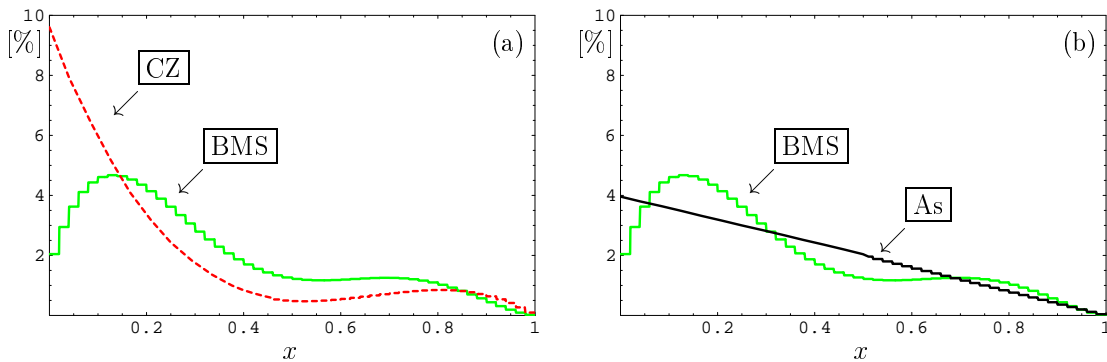


FIG. 3: Percentage distribution (see text) of the first inverse moment in x of the BMS model DA [1] in comparison with the CZ one [13] (a) and the asymptotic DA (b).

the endpoint regions. Even more, as Fig. 3 shows by plotting the first inverse moment $\langle x^{-1} \rangle_\pi$, calculated as $\int_x^{x+0.02} \varphi_\pi(x) x^{-1} dx$ and normalized to 100% (y -axis), the BMS DA receives in this region even less contributions than the asymptotic DA, as we explained above.

- By the same token, the Sudakov suppression of the endpoint region of the BMS DA is less crucial compared to endpoint-concentrated DAs. The implementation of Sudakov corrections using the analytic factorization scheme was considered in technical detail in [28] for the case of the asymptotic pion DA. Such an analysis for the BMS DA is more involved and will be conducted in a future publication.
- The deep reason for the failure of the CZ DA was provided in [65, 66, 89]. The condensate terms in the CZ sum rules are strongly peaked at the endpoints $x \rightarrow 0$ and $x \rightarrow 1$, the reason being that the vacuum quark distribution in the longitudinal momentum fractions is approximated by a $\delta(x)$ and its derivatives. For that reason, the condensate terms, i.e., the nonperturbative contributions to the sum rule, force the pion DA to be endpoint-concentrated, with the perturbative loop contribution proportional to $x(1-x)$ being insufficient to compensate these two sharp peaks at $x = 0$ and $x = 1$. Allowing for a smooth distribution in the longitudinal momentum for the vacuum quarks, i.e., using nonlocal condensates in the QCD sum rules (as done in the derivation of the BMS pion DA), the endpoint regions of the extracted DA are suppressed, despite the fact that its shape is doubly peaked.

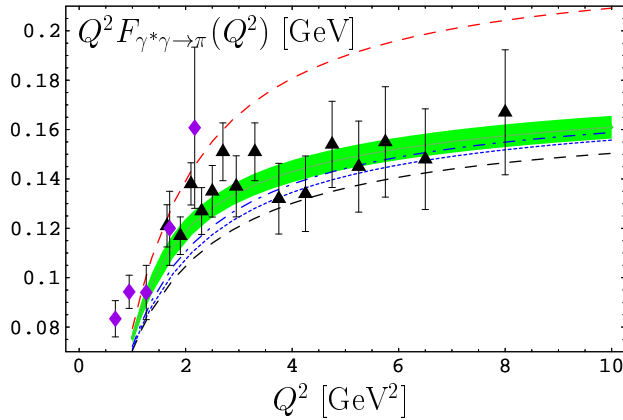


FIG. 4: Light-cone sum-rule predictions for $Q^2 F_{\gamma^* \gamma \rightarrow \pi}(Q^2)$ in comparison with the CELLO (diamonds, [90]) and the CLEO (triangles, [35]) experimental data evaluated with the twist-4 parameter value $\delta_{\text{Tw-4}}^2 = 0.19 \text{ GeV}^2$ [39, 40]. The predictions shown correspond to the following pion DA models: φ_{CZ} (upper dashed line) [13], BMS-“bunch” (shaded strip) [1], two instanton-based models, viz., [91] (dotted line) and [92] (dashed-dotted line), and the asymptotic pion DA φ_{as} (lower dashed line) [9, 11]. A recent transverse lattice result [93] is very close to the dash-dotted line, but starts to be closer to the center of the BMS strip for $Q^2 \geq 6 \text{ GeV}^2$.

- The endpoint behavior of the pion DA is the route cause why the pion-photon transition form factor—which in LO is purely electromagnetic—calculated with the CZ pion DA was found [43] to overshoot the CLEO data. More recently, the analysis of the CLEO data using light-cone sum rules [31, 38, 39, 40] has excluded the CZ pion

DA at the 4σ confidence level, while the BMS DA was found to be inside the 1σ error ellipse (for $\lambda_q^2 = 4 \text{ GeV}^2$), whereas even the asymptotic DA was also excluded by the CLEO data at the 3σ level. These quoted findings are reflected in the behavior of the predictions for the pion-photon transition form factor displayed in Fig. 4, which is based on the corrected version of [1] (the displayed strip is therefore slightly different from that in [47]).

To make these statements more transparent, let us define the DA profile deviation factor

$$\Delta_\varphi \equiv \frac{\langle x^{-1} \rangle_\pi^\varphi}{\langle x^{-1} \rangle_\pi^{\text{As}}} = 1 + a_2 + a_4 + \dots \quad (3.11)$$

which quantifies the deviation of a model DA from the asymptotic one and supply its value in Table I for several pion DAs suggested in the literature in comparison with the constraints from the experimental data and theoretical calculations. Reading this Table in conjunction with Fig. 4, one comes to the conclusion that the BMS “bunch” provides the best agreement with the CLEO and CELLO experimental constraints, being also in compliance with various theoretical constraints and lattice calculations.

TABLE I: Estimates for the Gegenbauer coefficients and the DA profile deviation factor Δ_φ up to polynomial order 4 for the asymptotic, the BMS, and the CZ DAs compared with constraints derived from light-cone sum rules (LCSR), QCD sum rules with nonlocal condensates (NL QCD SR) for the DA and the inverse moment $\langle x^{-1} \rangle$, ^a and by analyzing the CLEO data. Also shown are the corresponding entries for instanton-based models (ADT, PPRWG, PR) and those associated with a transverse-lattice calculation—labelled Lattice. All values displayed are normalized at the scale $\mu^2 = 1.35 \text{ GeV}^2$, corresponding to the scale of NL QCD SRs.

DA models/methods	a_2	a_4	$a_2 + a_4$	$a_2 - a_4$	Δ_φ
As	0	0	0	0	1
BMS	0.19	−0.13	0.06	0.32	1.06
CZ	0.52	0	0.52	0.52	1.52
PPRWG [91]	0.042	0.006	0.05	0.04	1.05
PR [134]	0.09	−0.02	0.07	0.10	1.07
ADT [94]	0.05	−0.04	0.01	0.09	1.01
Lattice [93]	0.08	0.02	0.10	0.06	1.10
LCSRs [33]	[0.07, 0.37]	—	—	—	1.22 ± 0.15
NL QCD SRs for DA [1]	[0.13, 0.25] ^a	[−0.04, −0.21] ^a	[+0.02, +0.09]	[+0.18, +0.46]	1.06 ± 0.04
NL QCD SR for $\langle x^{-1} \rangle$ [1]	—	—	[+0.00, +0.20]	—	1.10 ± 0.10
CLEO 1σ -limits [40]	[0.15, 0.43] ^a	[−0.60, −0.04] ^a	[−0.21, +0.15]	[+0.21, +1.00]	0.97 ± 0.18
CLEO 2σ -limits [40]	[0.11, 0.47] ^a	[−0.71, +0.07] ^a	[−0.31, +0.25]	[+0.07, +1.14]	0.97 ± 0.28
CLEO 3σ -limits [40]	[0.07, 0.51] ^a	[−0.82, +0.19] ^a	[−0.41, +0.35]	[−0.07, +1.28]	0.97 ± 0.38

^aNote that the uncertainties on the Gegenbauer coefficients a_2 and a_4 are correlated. Here, the rectangular limits of the fiducial ellipses extracted from the NL QCD SRs [1] and from the CLEO data in [39, 40] are shown.

B. Perturbative NLO evolution

Let us now discuss how the pion DA evolves at NLO using first standard perturbation theory to be followed by analogous considerations within APT. The evolution of the distribution amplitude (3.8) proceeds along the lines outlined in Appendix C. Taking into account only the first two Gegenbauer coefficients and LO evolution, one obtains

$$\varphi_\pi^{\text{LO}}(x, \mu_F^2) = 6x(1-x) \left[1 + a_2^{\text{D,LO}}(\mu_F^2) C_2^{3/2}(2x-1) + a_4^{\text{D,LO}}(\mu_F^2) C_4^{3/2}(2x-1) \right], \quad (3.12)$$

where $a_2^{\text{D,LO}}(\mu_F^2)$ and $a_4^{\text{D,LO}}(\mu_F^2)$ are given by (C18) taking recourse to (C14), and D denotes “diagonal”, while ND below stands for “nondiagonal”. On the other hand, the solution of

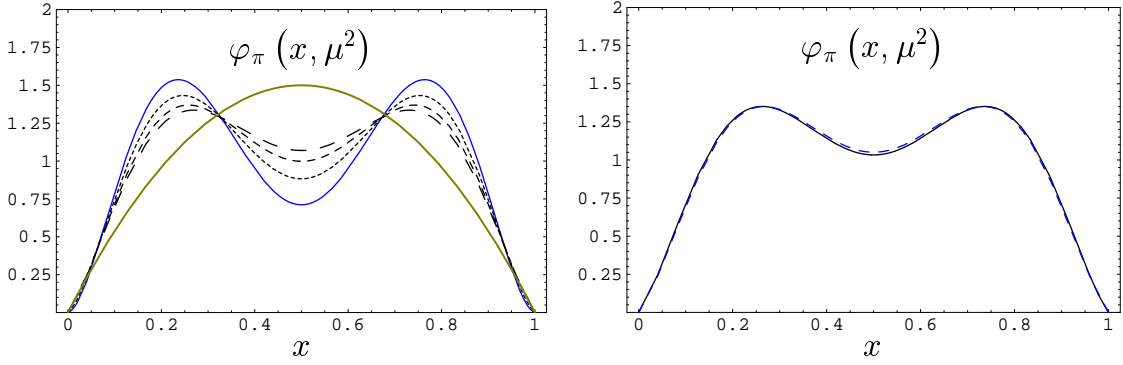


FIG. 5: The left panel shows the effect of the LO diagonal part of the evolution equation, Eq. (3.12), on the BMS DA. The convex solid line denotes the asymptotic profile of the pion DA, the other solid one stands for $\varphi_{\text{BMS}}^{\text{LO}}(x)$ at 1 GeV², while the broken lines represent $\varphi_{\text{BMS}}^{\text{LO}}(x)$ at 4, 20, and 100 GeV² (with the larger scale corresponding also to the larger value of the DA at the middle point). Right panel: Comparison of $\varphi_{\text{BMS}}^{\text{LO}}$ (Eq. (3.12)—solid line) and $\varphi_{\text{BMS}}^{\text{NLO}}$ (Eq. (3.13)—dashed line) at 20 GeV² to illustrate the effect of NLO evolution.

the NLO evolution equation takes the form

$$\varphi_\pi^{\text{NLO}}(x, \mu_F^2) = \varphi_\pi^{\text{D,NLO}}(x, \mu_F^2) + \frac{\alpha_s(\mu_F^2)}{4\pi} \varphi_\pi^{\text{ND,NLO}}(x, \mu_F^2), \quad (3.13a)$$

where

$$\varphi_\pi^{\text{D,NLO}}(x, \mu_F^2) = 6x(1-x) \left[1 + \sum_{n=2,4} a_n^{\text{D,NLO}}(\mu_F^2) C_n^{3/2}(2x-1) \right] \quad (3.13b)$$

and

$$\varphi_\pi^{\text{ND,NLO}}(x, \mu_F^2) = 6x(1-x) \sum_{n \geq 2}' a_n^{\text{ND,NLO}}(\mu_F^2) C_n^{3/2}(2x-1). \quad (3.13c)$$

The coefficients $a_n^{\text{D,NLO}}(\mu_F^2)$ and $a_n^{\text{ND,NLO}}(\mu_F^2)$ are given in (C19b) and (C19c), respectively, by employing (C15), while \sum' denotes the sum over even indices only. Note that, although the input DA, $\varphi_\pi(x, \mu_0^2)$, was parameterized by only two Gegenbauer coefficients a_2 and a_4 ,

higher harmonics also appear due to the nondiagonal nature of the NLO evolution.⁴ The effect of the inclusion of the LO diagonal part of the evolution kernel is important, as one sees from the left part of Fig. 5, which shows this effect for the BMS pion DA.

On the other hand, from the right part of Fig. 5, we deduce that the NLO nondiagonal evolution is rather small. We note that in the above computation the exact two-loop expression for α_s [95] in the $\overline{\text{MS}}$ -scheme ($\Lambda_{\text{QCD}} = 410$ MeV, $N_f = 3$) was employed, cf. (6.15), in which matching at the heavy-flavor thresholds $M_4 = 1.3$ GeV and $M_5 = 4.3$ GeV (with $M_1 = M_2 = M_3 = 0$) has been employed [96]. A discussion of the relation of this exact solution to the usual approximation, promoted by the Particle Data Group [86], has recently been given in [40] (see also Appendix C).

IV. PION FORM FACTOR AT NLO: ANALYTIC RESULTS

The NLO results for the hard-scattering amplitude T_H are summarized in Appendix A. Setting in (2.4) $\mu_F^2 = Q^2$ and taking into account the NLO evolution of the pion DA φ via (3.13), we obtain from (2.3)

$$F_\pi^{\text{Fact}}(Q^2; \mu_R^2) = F_\pi^{\text{LO}}(Q^2; \mu_R^2) + F_\pi^{\text{NLO}}(Q^2; \mu_R^2), \quad (4.1)$$

where the LO term is given by

$$F_\pi^{\text{LO}}(Q^2; \mu_R^2) = \alpha_s(\mu_R^2) \mathcal{F}_\pi^{\text{LO}}(Q^2) \quad (4.2)$$

$$Q^2 \mathcal{F}_\pi^{\text{LO}}(Q^2) \equiv 8 \pi f_\pi^2 \left[1 + a_2^{\text{D,NLO}}(Q^2) + a_4^{\text{D,NLO}}(Q^2) \right]^2 \quad (4.3)$$

and the calligraphic designations denote quantities with their α_s -dependence pulled out. In order to make a distinction between the contributions stemming from the diagonal and the nondiagonal parts of the NLO evolution equation of the pion DA, we express the NLO correction to the form factor in the form

$$F_\pi^{\text{NLO}}(Q^2; \mu_R^2) = \frac{\alpha_s^2(\mu_R^2)}{\pi} \left[\mathcal{F}_\pi^{\text{D,NLO}}(Q^2; \mu_R^2) + \mathcal{F}_\pi^{\text{ND,NLO}}(Q^2; N_{\text{Max}} = \infty) \right] \quad (4.4)$$

and write the diagonal contribution

$$\mathcal{F}_\pi^{\text{D,NLO}}(Q^2; \mu_R^2) \equiv b_0 \mathcal{F}_\pi^{(1,\beta)}(Q^2; \mu_R^2) + C_F \mathcal{F}_\pi^{(1,\text{F})}(Q^2) + C_G \mathcal{F}_\pi^{(1,\text{G})}(Q^2) \quad (4.5)$$

as a color decomposition (in correspondence with (A3)) in terms of

$$\begin{aligned} Q^2 \mathcal{F}_\pi^{(1,\beta)}(Q^2; \mu_R^2) &= 2 \pi f_\pi^2 \left[\frac{5}{3} + \frac{3 + (43/6)a_2^{\text{D,NLO}}(Q^2) + (136/15)a_4^{\text{D,NLO}}(Q^2)}{1 + a_2^{\text{D,NLO}}(Q^2) + a_4^{\text{D,NLO}}(Q^2)} - \ln \frac{Q^2}{\mu_R^2} \right] \\ &\times \left[1 + a_2^{\text{D,NLO}}(Q^2) + a_4^{\text{D,NLO}}(Q^2) \right]^2, \end{aligned} \quad (4.6a)$$

⁴ Since $a_n^{\text{ND,NLO}}(\mu_F^2)$ decreases with n , for the purpose of numerical calculations, we use an approximate form of $\varphi_{\text{ND}}^{\text{NLO}}(x, \mu_F^2)$ in which we neglect $a_n^{\text{ND,NLO}}(\mu_F^2)$ for $n > 100$.

$$Q^2 \mathcal{F}_\pi^{(1,F)}(Q^2) = 2\pi f_\pi^2 \left\{ -\frac{71}{6} - a_2^{\text{D,NLO}}(Q^2) \left[\frac{497}{36} - \frac{161}{24} a_2^{\text{D,NLO}}(Q^2) \right] \right. \\ \left. - a_4^{\text{D,NLO}}(Q^2) \left[\frac{1123}{450} - \frac{9793}{300} a_2^{\text{D,NLO}}(Q^2) - \frac{1387}{50} a_4^{\text{D,NLO}}(Q^2) \right] \right\} , \quad (4.6b)$$

and

$$Q^2 \mathcal{F}_\pi^{(1,G)}(Q^2) = 2\pi f_\pi^2 \left\{ -0.67 + a_2^{\text{D,NLO}}(Q^2) \left[18.70 + 16.35 a_2^{\text{D,NLO}}(Q^2) \right] \right. \\ \left. + a_4^{\text{D,NLO}}(Q^2) \left[24.23 + 36.76 a_2^{\text{D,NLO}}(Q^2) + 20.26 a_4^{\text{D,NLO}}(Q^2) \right] \right\} , \quad (4.6c)$$

where the superscripts F and G refer to the color factors C_F and $C_G = C_F - C_A/2$, respectively. Note that for the matter of calculational convenience, we also display the sum of these two terms (cf. Eq. (A7)):

$$Q^2 \mathcal{F}_\pi^{(1,FG)}(Q^2) = 2\pi f_\pi^2 \left\{ -15.67 - a_2^{\text{D,NLO}}(Q^2) \left[21.52 - 6.22 a_2^{\text{D,NLO}}(Q^2) \right] \right. \\ \left. - a_4^{\text{D,NLO}}(Q^2) \left[7.37 - 37.40 a_2^{\text{D,NLO}}(Q^2) - 33.61 a_4^{\text{D,NLO}}(Q^2) \right] \right\} . \quad (4.7)$$

On the other hand, the nondiagonal term reads

$$Q^2 \mathcal{F}_\pi^{\text{ND,NLO}}(Q^2; N_{\text{Max}}) = 4\pi f_\pi^2 \left[1 + a_2^{\text{D,NLO}}(Q^2) + a_4^{\text{D,NLO}}(Q^2) \right] \sum_{k=2}^{N_{\text{Max}}} 'a_k^{\text{ND,NLO}}(Q^2) , \quad (4.8)$$

where N_{Max} denotes the maximal number of Gegenbauer harmonics taken into account in order to achieve the desired accuracy.

As it was shown in Ref. [26], the effects of the LO DA evolution are crucial. In order to investigate the importance of the NLO DA evolution, we compare the predictions obtained using the complete NLO results, given above, with those derived by employing only the LO DA evolution via (3.12). The corresponding expressions in this latter case follow from those above by performing the replacements

$$a_n^{\text{D,NLO}} \rightarrow a_n^{\text{D,LO}} \quad \text{and} \quad a_n^{\text{ND,NLO}} \rightarrow 0 , \quad (4.9)$$

so that the contribution $\mathcal{F}_\pi^{\text{ND,NLO}}(Q^2; \mu_R^2)$ is absent. Introducing the notation

$$\tilde{\mathcal{F}}_\pi^i \equiv \mathcal{F}_\pi^i|_{\text{LO DA evolution}} , \quad (4.10)$$

we analyze the relative importance of the various contributions (LO, NLO, and Local Duality

(LD) part—see Sec. VII C) by defining the following ratios

$$R(Q^2, N_{\text{Max}}) = \frac{\mathcal{F}_\pi^{\text{LO}}(Q^2) + (\alpha_s/\pi)\mathcal{F}_\pi^{\text{ND,NLO}}(Q^2; N_{\text{Max}})}{\mathcal{F}_\pi^{\text{LO}}(Q^2) + (\alpha_s/\pi)\mathcal{F}_\pi^{\text{ND,NLO}}(Q^2; N_{\text{Max}} \approx \infty)}; \quad (4.11)$$

$$\hat{R}(Q^2, N_{\text{Max}}) = \frac{F_\pi^{\text{LD}}(Q^2) + \alpha_s \mathcal{F}_\pi^{\text{LO}}(Q^2) + (\alpha_s^2/\pi)\mathcal{F}_\pi^{\text{ND,NLO}}(Q^2; N_{\text{Max}})}{F_\pi^{\text{LD}}(Q^2) + \alpha_s \mathcal{F}_\pi^{\text{LO}}(Q^2) + (\alpha_s^2/\pi)\mathcal{F}_\pi^{\text{ND,NLO}}(Q^2; N_{\text{Max}} \approx \infty)}; \quad (4.12)$$

$$R_{\text{mod}}(Q^2) = \frac{\tilde{\mathcal{F}}_\pi^{\text{LO}}(Q^2)}{\mathcal{F}_\pi^{\text{LO}}(Q^2) + (\alpha_s/\pi)\mathcal{F}_\pi^{\text{ND,NLO}}(Q^2; N_{\text{Max}} \approx \infty)}; \quad (4.13)$$

$$\hat{R}_{\text{mod}}(Q^2) = \frac{F_\pi^{\text{LD}}(Q^2) + \alpha_s \tilde{\mathcal{F}}_\pi^{\text{LO}}(Q^2)}{F_\pi^{\text{LD}}(Q^2) + \alpha_s \mathcal{F}_\pi^{\text{LO}}(Q^2) + (\alpha_s^2/\pi)\mathcal{F}_\pi^{\text{ND,NLO}}(Q^2; N_{\text{Max}} \approx \infty)}. \quad (4.14)$$

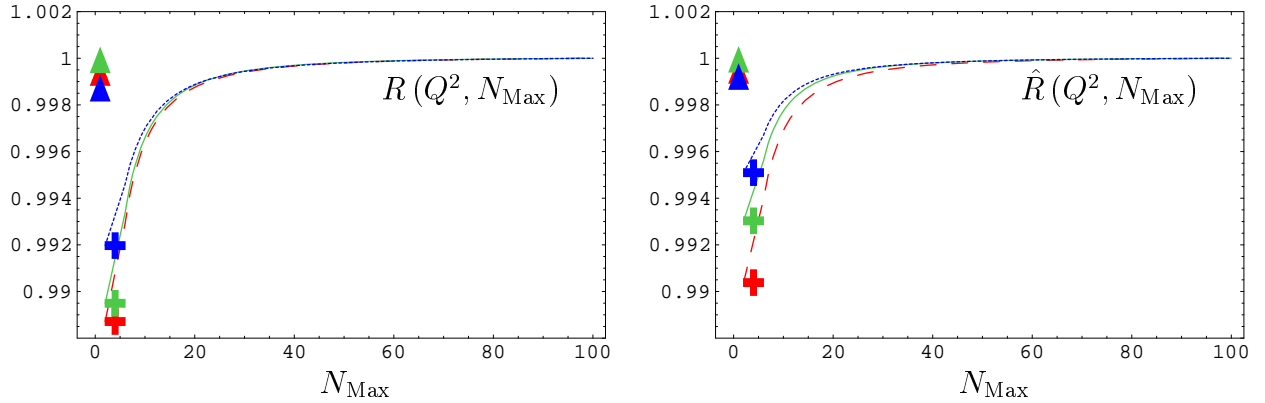


FIG. 6: Left: The ratio $R(Q^2, N_{\text{Max}})$, defined in Eq. (4.11), for three different values of Q^2 as a function of N_{Max} . The blue dotted curve corresponds to $Q^2 = 2 \text{ GeV}^2$, the green solid curve to $Q^2 = 10 \text{ GeV}^2$, and the red dashed one to $Q^2 = 50 \text{ GeV}^2$. Crosses of the same color represent the values of $R(Q^2, N_{\text{Max}} = 4)$, whereas triangles refer to $R_{\text{mod}}(Q^2)$, Eq. (4.13). Right: The same designations hold as for the left side, but now for the ratio $\hat{R}(Q^2, N_{\text{Max}})$ given by Eq. (4.12) and correspondingly for \hat{R}_{mod} —Eq. (4.14).

These ratios are displayed graphically in Fig. 6 for the BMS DA ($a_2(\mu_0^2) = 0.2$, $a_4(\mu_0^2) = -0.14$) in the region $N_{\text{Max}} = 4 - 100$. We infer from this figure that, adopting in our calculations an accuracy on the order of 99.5%, we can safely neglect the non-diagonal part of the NLO evolution equation and use for the pion form-factor computations to follow the approximate expression (omitting the superscript Approx)

$$F_\pi^{\text{Fact-Approx}}(Q^2; \mu_R^2) \equiv \alpha_s(\mu_R^2) \tilde{\mathcal{F}}_\pi^{\text{LO}}(Q^2; \mu_R^2) + \frac{\alpha_s^2(\mu_R^2)}{\pi} \mathcal{F}_\pi^{\text{D,NLO}}(Q^2; \mu_R^2). \quad (4.15)$$

Actually, the difference between $\mathcal{F}_\pi^{\text{D,NLO}}(Q^2; \mu_R^2)$ and $\tilde{\mathcal{F}}_\pi^{\text{D,NLO}}(Q^2; \mu_R^2)$ is of the order of $\alpha_s(Q^2)$, so that it is safe to use everywhere only the LO evolution. We have verified in our numerical calculations that the difference is indeed less than 1%.

V. SETTING THE RENORMALIZATION SCHEME AND SCALE

The choice of the expansion parameter represents the major ambiguity in the interpretation of the pQCD predictions because finite-order perturbative predictions depend unavoid-

ably on the renormalization scale and scheme choice.⁵ If one could optimize the choice of the renormalization scale and scheme according to some sensible criteria, the size of the higher-order corrections, as well as the size of the expansion parameter, i.e., the QCD running coupling, could serve as sensible indicators for the convergence of the perturbative expansion. In what follows, we shall consider several scheme and scale-setting options.

A. $\overline{\text{MS}}$ scheme

The results we have presented in the previous subsection were obtained in the $\overline{\text{MS}}$ renormalization (and factorization) scheme. Let us discuss the choice of the renormalization scale μ_R in some more detail. We see that in our NLO results, Eq. (4.4), this dependence is contained in the coupling constant $\alpha_s(\mu_R^2)$ as well as in the NLO correction $\mathcal{F}_\pi^{(1,\beta)}$. The latter correction is proportional to the b_0 coefficient of the β function and is N_f -dependent. Hence, a natural question arises: How can we determine the right value of N_f in the form-factor expression?

We propose here to apply the following procedures.

(i) The first one concerns the standard choice $\mu_R^2 = Q^2$ and suggests to shift μ_R^2 at the heavy-quark threshold in order to ensure the continuity of the form factor according to

$$F_\pi^{\text{Fact}}(Q^2) = \begin{cases} F_\pi^{\text{Fact}}(Q^2; \mu_R^2 = Q^2)|_{N_f=3} & \text{for } Q^2 \leq M_4^2; \\ F_\pi^{\text{Fact}}(Q^2; \mu_R^2 = Q^2 + \delta\mu_4^2)|_{N_f=4} & \text{for } \begin{cases} M_4^2 \leq Q^2 \\ Q^2 + \delta\mu_4^2 \leq M_5^2 \end{cases}; \\ F_\pi^{\text{Fact}}(Q^2; \mu_R^2 = Q^2 + \delta\mu_4^2 + \delta\mu_5^2)|_{N_f=5} & \text{for } M_5^2 \leq Q^2 + \delta\mu_4^2. \end{cases} \quad (5.1a)$$

As a result, we have to fulfill the following matching conditions

$$F_\pi^{\text{Fact}}(M_4^2; M_4^2)|_{N_f=3} = F_\pi^{\text{Fact}}(M_4^2; M_4^2 + \delta\mu_4^2)|_{N_f=4}; \quad (5.1b)$$

$$F_\pi^{\text{Fact}}(M_5^2 - \delta\mu_4^2; M_5^2)|_{N_f=4} = F_\pi^{\text{Fact}}(M_5^2 - \delta\mu_4^2; M_5^2 + \delta\mu_5^2)|_{N_f=5}. \quad (5.1c)$$

(ii) The second procedure addresses specifically the BLM scale setting $\mu_R^2 = \mu_{\text{BLM}}^2$. In this case, the only problem is the small value of the BLM scale (see Table II) due to the fact that the b_0 -term is completely absent and N_f -dependent terms do not arise. Therefore, we propose to implement the BLM scale setting only above some minimal scale: μ_{min} . Below this scale, which is in the range of the typical meson scales and hence only the light-quark sector ($N_f = 3$) contributes, we fix $\mu_R^2 = \mu_{\text{min}}^2$ and set $N_f = 3$ using the $\mathcal{F}_\pi^{(1,\beta)}(Q^2; \mu_{\text{min}}^2)$ -term in the form provided by (5.13)—more explanations will be given shortly.

The truncation of the perturbative series to a finite order introduces a residual dependence of the results on the scale μ_R , while the inclusion of higher-order corrections decreases this dependence. Nonetheless, we are still left with an intrinsic theoretical ambiguity of the perturbative results. One can try to estimate the uncertainty entailed by this ambiguity

⁵ Actually, to the order we are calculating these dependencies, they can be represented by a single parameter, say, the renormalization scale, because b_0 and b_1 are renormalization-scheme invariant.

(see, for example, [26]) or choose the renormalization scale μ_R on the basis of some physical arguments.

The simplest and widely used choice for μ_R is to identify it with the large external scale, i.e., to set

$$\mu_R^2 = Q^2, \quad (5.2)$$

the justification for adopting this choice being mainly a pragmatic one. However, physical arguments suggest that a more appropriate scale should be lower. Namely, since each external momentum entering an exclusive reaction is partitioned among many propagators of the underlying hard-scattering amplitude in the associated Feynman diagrams, the physical scales that control these processes are related to the average momentum flowing through the internal quark and gluon lines and are therefore inevitably softer than the overall momentum transfer. To treat this problem, several suggestions have been made in the literature. According to the so-called Fastest Apparent Convergence (FAC) procedure [97, 98], the scale μ_R is determined by the requirement that the NLO coefficient in the perturbative expansion of the physical quantity in question vanishes which here means

$$F_\pi^{\text{NLO}}(Q^2; \mu_R^2 = \mu_{\text{FAC}}^2) = 0. \quad (5.3)$$

On the other hand, following the Principle of Minimum Sensitivity (PMS) [99, 100, 101, 102], one mimics locally the global independence of the all-order expansion by choosing the renormalization scale μ_R to coincide with the stationary point of the truncated perturbative series. In our case, this reads

$$\left. \frac{d}{d\mu_R^2} [F_\pi^{\text{LO}}(Q^2; \mu_R^2) + F_\pi^{\text{NLO}}(Q^2; \mu_R^2)] \right|_{\mu_R^2 = \mu_{\text{PMS}}^2} = 0. \quad (5.4)$$

In the Brodsky–Lepage–Mackenzie (BLM) procedure [62], all vacuum-polarization effects from the QCD β -function (i.e., the effects of quark loops) are absorbed into the renormalized running coupling by resumming the large $(b_0\alpha_S)^n$ terms giving rise to infrared renormalons. According to the BLM procedure, the renormalization scale best suited to a particular process at a given order of expansion can be, in practice, determined by demanding that the terms proportional to the β -function should vanish. This naturally connects to conformal field theory and we refer the interested reader to [103] for a recent review. The optimization of the renormalization scale and scheme setting in exclusive processes by employing the BLM scale fixing was elaborated in [45] and in references cited therein. The renormalization scales in the BLM method are “physical” in the sense that they reflect the mean virtuality of the gluon propagators involved in the Feynman diagrams. According to the BLM procedure, the renormalization scale is determined by the condition

$$\mathcal{F}_\pi^{(1,\beta)}(Q^2; \mu_R^2 = \mu_{\text{BLM}}^2) = 0. \quad (5.5)$$

For calculational convenience, we express μ_R^2 in terms of Q^2 :

$$\mu_R^2 = a(Q^2) Q^2 \quad (5.6)$$

and proceed to calculate this quantity in the above-mentioned scale-setting schemes. Then,

TABLE II: Scales μ_{PMS} , μ_{FAC} , μ_{BLM} , and μ_V for the asymptotic, the BMS, and the CZ DAs.

DA	Q^2/μ_{FAC}^2	Q^2/μ_{PMS}^2	Q^2/μ_{BLM}^2	Q^2/μ_V^2	Q^2
As	18	27	106	20	any
BMS	16 – 20	24 – 29	105 – 117	20 – 22	1 – 50 GeV ²
CZ	146 – 62	217 – 92	475 – 278	90 – 52	1 – 50 GeV ²

the FAC procedure leads to

$$a_{\text{FAC}}(Q^2) = \exp \left[-\frac{5}{3} - \frac{3 + (43/6)a_2^{\text{D,NLO}}(Q^2) + (136/15)a_4^{\text{D,NLO}}(Q^2)}{1 + a_2^{\text{D,NLO}}(Q^2) + a_4^{\text{D,NLO}}(Q^2)} - \frac{4}{b_0} \frac{\mathcal{F}_\pi^{(1,\text{FG})}(Q^2) + \mathcal{F}_\pi^{\text{ND,NLO}}(Q^2)}{\mathcal{F}_\pi^{\text{LO}}(Q^2)} \right], \quad (5.7)$$

which can be related to the PMS procedure via

$$a_{\text{PMS}}(Q^2) = e^{-c_1/2} a_{\text{FAC}}(Q^2) \quad (5.8)$$

with $c_1 \equiv b_1/b_0^2$. This value corresponds to the stationary point (the maximum) of the NLO prediction for F_π^{Fact} .

On the other hand, for the BLM scale one obtains

$$\mu_{\text{BLM}}^2 = a_{\text{BLM}}(Q^2) Q^2, \quad (5.9a)$$

where

$$a_{\text{BLM}}(Q^2) = \exp \left[-\frac{5}{3} - \frac{3 + (43/6)a_2^{\text{D,NLO}}(Q^2) + (136/15)a_4^{\text{D,NLO}}(Q^2)}{1 + a_2^{\text{D,NLO}}(Q^2) + a_4^{\text{D,NLO}}(Q^2)} \right]. \quad (5.9b)$$

The values of the scales μ_{PMS} , μ_{FAC} , and μ_{BLM} for the asymptotic, the CZ, and the BMS DAs, defined in (3.10), are listed in Table II. One notices that the BLM scale is rather low for all considered DAs. This makes its applicability at experimentally accessible Q^2 values rather questionable. But it is possible to improve this scale-setting procedure in the following way.

First of all, let us rewrite the BLM prescription in the more suggestive form

$$\left\{ F_\pi(Q^2; \mu_R^2), \mathcal{F}_\pi^{(1,\beta)}(Q^2; \mu_R^2) = \frac{1}{4} \mathcal{F}_\pi^{\text{LO}}(Q^2) \ln \left[\frac{\mu_R^2}{\mu_{\text{BLM}}^2(Q^2)} \right] \right\} \xrightarrow{\text{BLM}} \left\{ F_\pi(Q^2; \mu_{\text{BLM}}^2(Q^2)), \mathcal{F}_\pi^{(1,\beta)}(Q^2; \mu_{\text{BLM}}^2(Q^2)) = 0 \right\}. \quad (5.10)$$

It becomes evident that when the BLM scale yields α_s values close to unity, perturbation theory breaks down. To avoid this happening, one can, of course, introduce ad hoc a cutoff for α_s , operative, say, above 0.5 – 0.6, or one can “freeze” α_s at low Q^2 scales to some finite

value by introducing an effective gluon mass [45, 63].⁶ Still another possibility is to use the analytic coupling [56], as done in [28, 29] (see next section).

In order to protect the BLM scale from intruding into the forbidden nonperturbative soft region, where perturbation theory becomes invalid, one can make use of a minimum scale, μ_{\min} , based on the grounds of QCD factorization theorems and the OPE, as applied for instance in [104, 105, 106, 107] and also in [32]:

$$\mu_{\min}^2 \geq \mu_0^2. \quad (5.11)$$

Here μ_0^2 stands for a typical nonperturbative (hadronic) scale in the range $[0.4-1.5] \text{ GeV}^2$ and corresponds roughly to the inverse distance at which the parton and hadron representations have to match each other. Note that the smaller μ_{\min}^2 is chosen, the deeper the endpoint region $x \rightarrow 1$ can be explored for smaller values of Q^2 . It is intuitively clear that the typical parton virtuality in the (hard) Feynman diagrams—let us call it μ_q^2 —should not become less than its counterpart in the pion bound state: μ_π^2 . Because the latter is linked to the scale μ_0^2 , the scale μ_{\min}^2 should be limited from below by this scale. Consequently, we assume that the following hierarchy of scales—partonic (i.e., perturbative) and hadronic (i.e., nonperturbative)—holds:

$$\lambda_q^2 < \mu_0^2 \leq \mu_q^2 \leq \mu_{\text{R-scheme}}^2. \quad (5.12)$$

Then, if $\mu_{\text{BLM}}^2 < \mu_0^2$, one obtains instead of Eq. (5.10), the IR protected version (termed in our analysis $\overline{\text{BLM}}$ prescription)

$$\left\{ F_\pi [Q^2, \mu_{\text{BLM}}^2(Q^2)], \mathcal{F}_\pi^{(1,\beta)} [Q^2, \mu_{\text{BLM}}^2(Q^2)] = 0 \right\} \xrightarrow{\overline{\text{BLM}}} \left\{ F_\pi(Q^2; \mu_{\min}^2), \mathcal{F}_\pi^{(1,\beta)}(Q^2; \mu_{\min}^2) = \frac{1}{4} \mathcal{F}_\pi^{\text{LO}}(Q^2) \ln \left(\frac{\mu_{\min}^2}{\mu_{\text{BLM}}^2(Q^2)} \right) \right\}. \quad (5.13)$$

This modification of the BLM scale setting enables us to treat the problem of the N_f -dependence of the β function in the term $\mathcal{F}_\pi^{(1,\beta)}(Q^2; \mu_{\text{R}}^2)$ without any further assumptions or modifications. Because of the fact that the scale μ_{R}^2 is now bounded from below by (5.11), one is not faced with ambiguities related to the variation of the number of active flavors N_f due to heavy-quark thresholds in the b_0 coefficient entering $\mathcal{F}_\pi^{(1,\beta)}(Q^2; \mu_{\text{R}}^2)$. According to this, we set $N_f = 3$ for $\mu_{\text{R}}^2 = \mu_{\min}^2$, whereas for $\mu_{\text{R}}^2 = \mu_{\text{BLM}}^2 > \mu_{\min}^2$ there is no ambiguity by virtue of $\mathcal{F}_\pi^{(1,\beta)}(Q^2; \mu_{\text{BLM}}^2) = 0$. Therefore, the bona fide BLM scale setting reads

$$\mu_{\overline{\text{BLM}}} = \max \{ \mu_{\text{BLM}}, \mu_{\min} \}, \quad (5.14)$$

where μ_{\min} will be specified later on in connection with the soft part of the form factor.

B. α_V scheme

The self-consistency of perturbation theory implies that the difference in the calculation to order n of the same physical quantity in two different schemes must be of order $n + 1$.

⁶ Restricting the value of α_s does not necessarily limit the quark and gluon virtualities in the Feynman diagrams to values for which perturbation theory applies.

This means that relations among different physical observables must be independent of the renormalization scale and scheme conventions to any fixed order of perturbation theory. In Ref. [108] it was argued that by applying the BLM scale-fixing procedure to perturbative predictions of two observables in, for example, the $\overline{\text{MS}}$ -scheme, and then algebraically eliminating $\alpha_{\overline{\text{MS}}}$, one can link to each other any perturbatively calculable observables without scale and scheme ambiguity. Within this approach, the choice of the BLM scale ensures that the resulting “commensurate scale relation” is independent of the choice of the intermediate renormalization scheme employed. On these grounds, Brodsky *et al.* in [45] have analyzed several exclusive hadronic amplitudes in the α_V scheme, in which the effective coupling $\alpha_V(\mu^2)$ is defined by utilizing the heavy-quark potential $V(\mu^2)$. The α_V scheme is a “natural”, physically motivated scheme, which by definition, automatically incorporates vacuum polarization effects due to the fermion-antifermion pairs into the coupling. The μ_V^2 scale which then appears in the argument of the α_V coupling reflects the mean virtuality of the exchanged gluons. Furthermore, since α_V is an effective running coupling defined by virtue of a physical quantity, it must be *finite* at low momenta, and, therefore, an appropriate parameterization of the low-energy region should, in principle, be included.

The scale-fixed relation between the couplings $\alpha_{\overline{\text{MS}}}$ and α_V is given by [45]

$$\alpha_s(\mu_{\text{BLM}}^2) = \alpha_V(\mu_V^2) \left[1 + \frac{\alpha_V(\mu_V^2)}{4\pi} \frac{8C_A}{3} + \dots \right], \quad (5.15a)$$

where

$$\mu_V^2 = e^{5/3} \mu_{\text{BLM}}^2. \quad (5.15b)$$

The scales μ_V associated with selected pion DAs are included in Table II.

Taking into account Eqs. (5.15), the NLO prediction for the pion form factor, given by Eqs. (4.1)–(4.8), gets modified as follows

$$\begin{aligned} \alpha_s(\mu_R^2) &\rightarrow \alpha_V(\mu_V^2) \\ \mathcal{F}_\pi^{\text{D,NLO}}(Q^2) &\rightarrow \mathcal{F}_\pi^{\text{D,NLO}}(Q^2) = \mathcal{F}_\pi^{(1,\text{FG})}(Q^2) + 2\mathcal{F}_\pi^{\text{LO}}(Q^2). \end{aligned} \quad (5.16)$$

We are not going to present predictions in this scheme using the standard QCD coupling, as this would require the introduction of exogenous parameters, like an effective gluon mass, that cannot be fixed within the same approach but have to be taken from elsewhere. For such an application, we refer the interested reader to the analysis of [45]. The connection of [45] to the analytic approach, which we will use below, was discussed in detail in [29]. Predictions for the pion form factor within the α_V scheme will be presented below in the context of Analytic Perturbation Theory.

VI. STRONG RUNNING COUPLING AND NON-POWER SERIES EXPANSIONS

A. One-loop case

In the one-loop approximation we have a rather simple renormalization-group (RG) equation for the running coupling constant:

$$\frac{d \alpha_s(\mu^2)}{d \ln \mu^2} = \beta(\mu^2); \quad (6.1)$$

$$\beta_{1\text{-loop}}(\mu^2) = -b_0 \left(\frac{\alpha_s^2(\mu^2)}{4\pi} \right) \quad (6.2)$$

with b_0 given in Appendix A. The solution of this equation has the form

$$\alpha_s^{(1)}(Q^2) = \frac{4\pi}{b_0 \ln(Q^2/\Lambda^2)}, \quad (6.3)$$

where $\Lambda \equiv \Lambda_{\text{QCD}}$ is the QCD scale parameter. A well-known problem here is the appearance of an IR pole at $Q^2 = \Lambda^2$, which spoils the analyticity of the QCD running coupling.

In a series of papers [2, 56, 109, 110] Shirkov and Solovtsov introduced an analytic running coupling that avoids by construction the Landau singularity, thus generalizing earlier attempts by Radyushkin [111] and Krasnikov and Pivovarov [112]. To this end, they used the spectral representation for the QCD running coupling $\bar{\alpha}_s(Q^2)$ (the bar over α_s means that the analyticity property is valid) and expressed it in the form

$$\bar{\alpha}_s(Q^2) = \frac{1}{\pi} \int_0^\infty d\sigma \frac{\rho(\sigma)}{\sigma + Q^2 - i\epsilon} \quad (6.4)$$

without subtractions due to the fact that the spectral density $\rho(\sigma)$ decreases as $1/\ln^2 \sigma$ for large σ . The corresponding one-loop spectral density reads

$$\rho^{(1)}(\sigma) = \left(\frac{4\pi}{b_0} \right) \frac{\pi}{\ln^2(\sigma/\Lambda^2) + \pi^2} \quad (6.5)$$

and provides the one-loop singularity-free coupling function

$$\bar{\alpha}_s^{(1)}(Q^2/\Lambda^2) = \frac{4\pi}{b_0} \left[\frac{1}{\ln(Q^2/\Lambda^2)} + \frac{\Lambda^2}{\Lambda^2 - Q^2} \right]. \quad (6.6)$$

The first term on the RHS expresses the standard UV behavior of the invariant coupling, while the second one compensates the ghost pole at $Q^2 = \Lambda^2$ and has a nonperturbative origin, being suppressed at $Q^2 \rightarrow \infty$.

Let us now consider powers of the analytic coupling function. By performing an analytic continuation of the k -th power of the function (6.3) in the complex Q^2 -plane, one determines the corresponding spectral functions $\rho_k^{(1)}(\sigma)$, ($k = 1, 2 \dots$):

$$\rho_k^{(1)}(\sigma) = \left(\frac{4\pi}{b_0} \right)^k \text{Im} \left(\frac{1}{\ln(-\sigma/\Lambda^2)} \right)^k, \quad (6.7)$$

which in turn determine the analytic image $\mathcal{A}_k^{(1)}(Q^2)$ of $[\alpha_s^{(1)}(Q^2)]^k$, i.e.,

$$\mathcal{A}_k^{(1)}(Q^2) = \frac{1}{\pi} \int_0^\infty d\sigma \frac{\rho_k^{(1)}(\sigma)}{\sigma + Q^2 - i\epsilon}. \quad (6.8)$$

For $k = 1, 2, \dots$, we have

$$\mathcal{A}_{k+1}^{(1)}(Q^2) = - \left(\frac{4\pi}{kb_0} \right) \frac{\partial \mathcal{A}_k^{(1)}(Q^2)}{\partial \ln Q^2} \quad \text{and} \quad \mathcal{A}_1^{(1)}(Q^2) \equiv \bar{\alpha}_s^{(1)}(Q^2/\Lambda^2), \quad (6.9)$$

which for $k = 1$ reduces to

$$\mathcal{A}_2^{(1)}(Q^2) = \left(\frac{4\pi}{b_0} \right)^2 \left[\frac{1}{\ln^2(Q^2/\Lambda^2)} + \frac{Q^2 \Lambda^2}{(\Lambda^2 - Q^2)^2} \right]. \quad (6.10)$$

Notice at this point some key properties of these functions:

- each $\mathcal{A}_k^{(1)}(Q^2)$ with $k \geq 2$ tends to zero for $Q^2 \rightarrow 0$;
- each $\mathcal{A}_k^{(1)}(Q^2)$ has exactly $k - 1$ zeros for $Q^2 \in [0, \infty)$;
- when $Q^2 \rightarrow \infty$, each $\mathcal{A}_k^{(1)}(Q^2) \Big|_{Q^2 \rightarrow \infty} \sim 1/\ln^k[Q^2]$ tends to 0.

These properties are universal in the sense that they do not depend on the loop order. The functions $\mathcal{A}_k(Q^2)$ are used in the so-called Analytic Perturbation Theory [2, 3, 6, 56, 57, 58], where standard perturbative series, for example, for the Adler function

$$D^{\text{PT}}(Q^2) = N_c \sum_f e_f^2 \left\{ 1 + \frac{\alpha_s(Q^2)}{\pi} + d_1 \left[\frac{\alpha_s(Q^2)}{\pi} \right]^2 + \dots \right\} \quad (6.11)$$

is recast into a non-power series expansion to obtain

$$D^{\text{APT}}(Q^2) = N_c \sum_f e_f^2 \left[1 + \frac{\mathcal{A}_1(Q^2)}{\pi} + d_1 \frac{\mathcal{A}_2(Q^2)}{\pi^2} + \dots \right]. \quad (6.12)$$

The one-loop expressions for \mathcal{A}_1 and \mathcal{A}_2 are given in (6.9) and (6.10), respectively.

B. Two-loop case

In the two-loop case the situation is more complicated. The corresponding β -function reads

$$\beta_{2\text{-loop}}(\alpha) = \frac{-b_0 \alpha^2}{4\pi} \left(1 + \frac{b_1 \alpha}{b_0 4\pi} \right) \quad (6.13)$$

with the first two beta coefficients given in Appendix A. Integrating the RG equation (6.1), we obtain the transcendental equation

$$L_Q = \frac{4\pi}{\alpha(L_Q) b_0} - c_1 \ln \left(c_1 + \frac{4\pi}{\alpha(L_Q) b_0} \right), \quad c_1 = \frac{b_1}{b_0^2}, \quad L_Q \equiv \ln(Q^2/\Lambda^2). \quad (6.14)$$

As has been shown in [95], the two-loop running coupling in QCD, being the solution of this equation, can be written via the Lambert W_{-1} function

$$\alpha_s^{(2)}(Q^2) = -\frac{4\pi}{b_0 c_1} \left[1 + W_{-1} \left(-\frac{1}{c_1 e} \left(\frac{\Lambda^2}{Q^2} \right)^{1/c_1} \right) \right]^{-1}. \quad (6.15)$$

For some more explanations we refer the interested reader to [39], Appendix C, Eqs. (C15) and (C20) in conjunction with figure 5. By performing the analytic continuation of function (6.15) in the complex Q^2 -plane, the spectral function $\rho^{(2)}(\sigma)$ can be determined [113]:

$$\rho^{(2)}(\sigma) = \frac{4\pi}{b_0 c_1} \mathbf{Im} \left(-\frac{1}{1 + W_1(z(\sigma))} \right), \quad (6.16)$$

where

$$z(\sigma) = \frac{1}{c_1 e} \exp[-\sigma/c_1 + i(1/c_1 - 1)\pi]. \quad (6.17)$$

Then, the analytic coupling $\bar{\alpha}_s^{(2)}(Q^2)$ in the 2-loop approximation becomes

$$\bar{\alpha}_s^{(2)}(Q^2) = \frac{1}{\pi} \int_0^\infty d\sigma \frac{\rho^{(2)}(\sigma)}{\sigma + Q^2 - i\epsilon}. \quad (6.18)$$

However, this expression is too complex to be treated exactly. For that reason, Shirkov and Solovtsov suggested in [2] to use instead the approximate expression

$$\bar{\alpha}_s^{(2,\text{approx})}(Q^2) = \frac{4\pi}{b_0} \bar{a}_s[\ell(L_Q, c_1)], \quad (6.19)$$

$$\bar{a}_s(\ell) \equiv \frac{1}{\ell} + \frac{1}{1 - \exp(\ell)}, \quad \ell(L_Q, c) \equiv L_Q + c \ln \sqrt{L_Q^2 + 4\pi^2} \quad (6.20)$$

with the same L_Q as in (6.14). This expression reproduces both the UV two-loop asymptotic behavior as well as the value at the infrared fixed point $Q^2 = 0$ rather well. More specifically, above about $Q^2 \geq 1 \text{ GeV}^2$, it resembles the exact result with an accuracy in the range of 99% and can be used for all higher Q^2 values. Note in this context that the one-loop expression $\bar{\alpha}_s^{(1)}(Q^2)$, Eq. (6.3), can be represented by

$$\bar{\alpha}_s^{(1)}(Q^2) = \frac{4\pi}{b_0} \bar{a}_s(L_Q). \quad (6.21)$$

The only feature not yet taken into account in the above approximation is the matching at the quark-flavor thresholds: $M_4 = 1.3 \text{ GeV}$, $M_5 = 4.3 \text{ GeV}$, and $M_6 = 170 \text{ GeV}$ (with $M_1 = M_2 = M_3 = 0$). However, taking into account this matching, the approximate formula (6.19) starts to become inaccurate. As a result of the interpolation procedure, we obtain then in this (so-called “global” fit in the Shirkov–Solovtsov terminology [4]—abbreviated by the self-explaining label “fit”) case another approximation:⁷

$$\bar{\alpha}_s^{(2,\text{fit})}(Q^2) = \frac{4\pi}{b_0(N_f = 3)} \bar{a}_s \left[\ell \left(\ln \frac{Q^2}{\Lambda_{21}^2}, c_{21}^{\text{fit}} \right) \right], \quad (6.22)$$

⁷ This interpolation is based upon data contained in [113, 114] and also on unpublished data provided to us by B. A. Magradze.

TABLE III: Parameters entering Eq. (6.22) for different values of the QCD scale parameter $\Lambda_{\text{QCD}}^{N_f=3}$.

Parameters	$\Lambda_{\text{QCD}}^{N_f=3} = 350 \text{ MeV}$	$\Lambda_{\text{QCD}}^{N_f=3} = 400 \text{ MeV}$	$\Lambda_{\text{QCD}}^{N_f=3} = 450 \text{ MeV}$
c_{21}^{fit}	-1.012	-1.015	-1.091
Λ_{21}	57 MeV	67 MeV	69 MeV
$\ln(\Lambda_{21}^2/1 \text{ GeV}^2)$	-5.738	-5.412	-5.349

with the parameters c_{21}^{fit} and Λ_{21} listed in Table III. The quality of this approximation ensures a deviation less than 1% in the whole Q^2 interval and is illustrated in Fig. 7.

To fix the parameter $\Lambda_{\text{QCD}}^{N_f=3}$, we use [86]

$$\bar{\alpha}_s^{(2)}(m_Z^2) = 0.120 \quad (6.23)$$

that gives us

$$\Lambda_{\text{QCD}}^{N_f=3} = 400 \text{ MeV}. \quad (6.24)$$

Let us now focus our attention to powers of the analytic coupling function. By performing the analytic continuation of the k -th power of function (6.15) in the complex Q^2 -plane, one determines the corresponding spectral functions $\rho_k^{(2)}(\sigma)$, $k = 1, 2 \dots$:

$$\rho_k^{(2)}(t) = \left(\frac{4\pi}{b_0 c_1} \right)^k \text{Im} \left(-\frac{1}{1 + W_1(z(t))} \right)^k, \quad (6.25)$$

which in turn provide the analytic images $\mathcal{A}_k^{(2)}(Q^2)$ of $[\alpha_s^{(2)}(Q^2)]^k$; viz.,

$$\mathcal{A}_k^{(2)}(Q^2) = \frac{1}{\pi} \int_0^\infty d\sigma \frac{\rho_k^{(2)}(\sigma)}{\sigma + Q^2 - i\epsilon}. \quad (6.26)$$

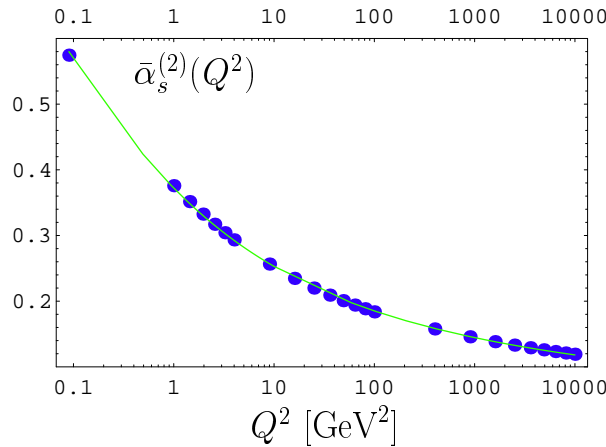


FIG. 7: The solid line shows the approximate expression, given by $\bar{\alpha}_s^{(2,\text{fit})}(Q^2)$, Eq. (6.22), whereas the bullets represent the exact values of $\bar{\alpha}_s^{(2)}(Q^2)$ taking into account heavy-quark threshold matching.

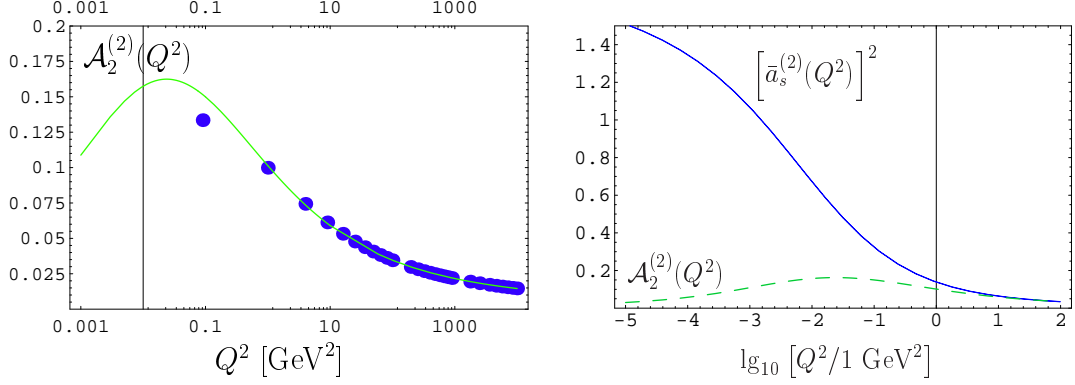


FIG. 8: (Left) The solid line represents the approximate expression $\mathcal{A}_2^{(2,\text{fit})}(Q^2)$ given by Eq. (6.28), whereas the bullets denote the exact values of $\mathcal{A}_2^{(2)}(Q^2)$ taking into account the heavy-quark threshold matching. (Right) Comparison of $\mathcal{A}_2^{(2,\text{fit})}(Q^2)$ (dashed curve) with $[\bar{\alpha}_s^{(2,\text{fit})}(Q^2)]^2$ (solid curve). Note the modified scale of the abscissa.

These functions obey a more complicated recurrence relation: ($k = 1, 2 \dots$)

$$\frac{\partial \mathcal{A}_k^{(2)}(Q^2)}{\partial \ln Q^2} = -k \frac{b_0}{4\pi} \left[\mathcal{A}_{k+1}^{(2)}(Q^2) + \frac{b_1}{4\pi b_0} \mathcal{A}_{k+2}^{(2)}(Q^2) \right] \quad \text{and} \quad \mathcal{A}_1^{(2)}(Q^2) \equiv \bar{\alpha}_s^{(2)}(Q^2/\Lambda^2). \quad (6.27)$$

As a result of the interpolation procedure, we obtain in the “global” case the following approximation for $k = 2$

$$\mathcal{A}_2^{(2,\text{fit})}(Q^2) = \left[\frac{4\pi}{b_0(N_f = 3)} \right]^2 \left\{ \frac{1}{L^2} - \frac{\exp(L)}{[1 - \exp(L)]^2} \right\}_{L=\ell \left[\ln \left(\frac{Q^2}{\Lambda_{22}^2} \right), c_{22}^{\text{fit}} \right]}, \quad (6.28)$$

with the parameters c_{22}^{fit} and Λ_{22} being listed in Table IV. The quality of the approximation is high with the deviation restricted to about 1% (10%) for $Q^2 \geq 1 \text{ GeV}^2$ ($Q^2 \leq 0.1 \text{ GeV}^2$), as illustrated in Fig. 8. One sees from this figure that for $Q^2 \geq 10 \text{ GeV}^2$ the difference between the exact and approximate expression starts to be negligible with the sizable deviation being confined in the region $Q^2 \leq 1 \text{ GeV}^2$.

C. Factorization of the pion form factor at NLO under analytization

The analytization procedure of the pion form factor at NLO leads to ambiguities, first discussed in [29]. The key question is: according to what analytization prescription are we

TABLE IV: Parameters entering Eq. (6.28) for different values of the QCD scale parameter $\Lambda_{\text{QCD}}^{N_f=3}$.

Parameters	$\Lambda_{\text{QCD}}^{N_f=3} = 350 \text{ MeV}$	$\Lambda_{\text{QCD}}^{N_f=3} = 400 \text{ MeV}$	$\Lambda_{\text{QCD}}^{N_f=3} = 450 \text{ MeV}$
c_{22}^{fit}	-1.549	-1.544	-1.534
Λ_{22}	29 MeV	34.5 MeV	41 MeV
$\ln(\Lambda_{22}^2/1 \text{ GeV}^2)$	-7.088	-6.734	-6.399

replacing the running strong coupling and its powers by their analytic images? In fact, it is possible to impose the analytization of the NLO term of F_π^{Fact} following two different main options:

- In keeping with our philosophy of the analytization of observables as a whole [60, 61], we may adopt a *Maximally Analytic* prescription and use in the NLO term of the pion form factor also the analytic image of α_s^2 . This amounts to

$$[F_\pi^{\text{Fact}}(Q^2; \mu_R^2)]_{\text{MaxAn}} = \bar{\alpha}_s^{(2)}(\mu_R^2) \mathcal{F}_\pi^{\text{LO}}(Q^2) + \frac{1}{\pi} \mathcal{A}_2^{(2)}(\mu_R^2) \mathcal{F}_\pi^{\text{NLO}}(Q^2; \mu_R^2), \quad (6.29a)$$

which will be evaluated with the aid of Eq. (6.28).

- Another procedure, we call *Naive Analytic*, replaces the strong coupling and its powers by the analytic coupling $\bar{\alpha}_s$ and its powers $\bar{\alpha}_s^2$ everywhere in the NLO term of F_π^{Fact} . This is actually the analytization procedure proposed in [29] and amounts to the following requirement

$$[F_\pi^{\text{Fact}}(Q^2; \mu_R^2)]_{\text{NaivAn}} = \bar{\alpha}_s^{(2)}(\mu_R^2) \mathcal{F}_\pi^{\text{LO}}(Q^2) + \frac{1}{\pi} [\bar{\alpha}_s^{(2)}(\mu_R^2)]^2 \mathcal{F}_\pi^{\text{NLO}}(Q^2; \mu_R^2). \quad (6.29b)$$

Note that the naive analytization does not respect nonlinear relations of the coupling owing to different dispersive images.

Anticipating our detailed numerical analysis of the pion form factor using APT, we define

$$\Delta F_\pi^{\text{an}}(Q^2) \equiv [F_\pi^{\text{Fact}}(Q^2)]_{\text{MaxAn}} - [F_\pi^{\text{Fact}}(Q^2)]_{\text{NaivAn}}, \quad (6.30)$$

which provides a quantitative measure for the analytization ambiguity.

VII. PION FORM FACTOR AT NLO: NUMERICAL ANALYSIS AND COMPARISON WITH EXPERIMENTAL DATA

In this section we would like to present our predictions for the pion form factor utilizing the BMS pion DA and pQCD at the level of NLO accuracy. First, we consider the standard perturbative approach with different scale settings within the $\overline{\text{MS}}$ scheme and continue then with a detailed discussion of the pion form factor as a non-power series expansion of the QCD analytic coupling. To this end, we employ the analytization procedures discussed before to obtain $Q^2 F_\pi^{\text{Fact}}$ in the $\overline{\text{MS}}$ scheme, with different scale settings, and also in the α_V scheme. To confront our theoretical predictions with the experimental data in the last subsection, we will include the soft non-factorizable contribution, modelled on the basis of local duality. To join properly the hard and soft contributions, local duality and the Ward identity at $Q^2 = 0$ will be employed in order to ensure that each of these contributions is evaluated in its own region of validity, according to the factorization of the parton and hadron representations. A comparison of these predictions with the corresponding ones obtained with the asymptotic pion DA will be included.

A. Standard perturbative approach

As outlined in Sec. V, the NLO prediction for the pion form factor, as any other finite-order prediction, contains a theoretical uncertainty stemming from its dependence on the renormalization scale μ_R and the scheme used. This dependence is, however, reduced in comparison with the LO prediction due to the inclusion of the NLO correction. To quantify these statements, we plot in Fig. 9(a) the ratio $R_{\text{NLO}}(Q^2) = F_{\pi}^{\text{NLO}}(Q^2)/F_{\pi}^{\text{LO}}(Q^2)$ and in Fig. 9(b) the result for the factorized form factor at NLO, using the BMS DA in the $\overline{\text{MS}}$ scheme with different scale settings. The main observation from these figures is the strong sensitivity of $R_{\text{NLO}}(Q^2)$ and the moderate dependence of $F_{\pi}^{\text{Fact}}(Q^2)$ on the scale-setting procedure adopted—especially at Q^2 values accessible to present experiments.

Let us discuss these figures in a systematic way.

- For $\mu_R^2 = Q^2$, the ratio $R_{\text{NLO}}(Q^2)$ is positive, large (on the order of about 50%) and decreases very slowly, while α_s is small (~ 0.3). As a result, the LO contribution is about twice as the NLO one and the form factor is small.
- Using the FAC scale setting, the whole NLO contribution vanishes, so that also the ratio is zero. In this case, the form factor is rather moderate down to momenta of the order of 10 GeV², where the QCD effective coupling becomes of order unity.
- Applying the PMS scale setting, the NLO contribution is negative with $R_{\text{NLO}}(Q^2)$ being small and also negative down to a critical value of $Q^2 \simeq 6$ GeV² (see Table II), where the absolute value of the NLO contribution becomes equal to the LO one and the form factor becomes zero. For this scale setting, already at $Q^2 \simeq 6$ GeV², the QCD effective coupling starts “feeling” the Landau singularity and becomes excessively large, while above 10 GeV² the form factor is rather moderate.
- Adopting the BLM procedure, the results are quite similar to those obtained with the PMS scale setting with respect to the ratio $R_{\text{NLO}}(Q^2)$, whereas the form factor now is

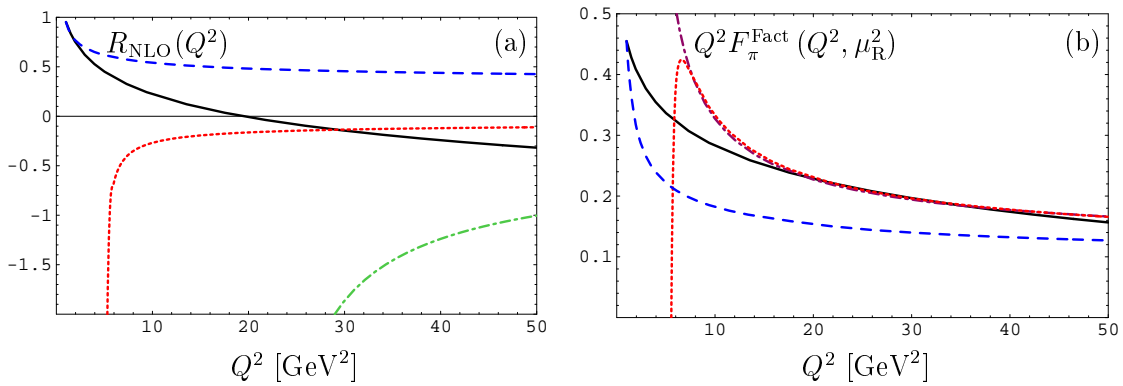


FIG. 9: The ratio $R_{\text{NLO}}(Q^2)$, (a), and the NLO results for $Q^2 F_{\pi}^{\text{Fact}}$, (b), in the $\overline{\text{MS}}$ scheme with various renormalization scale settings. The dashed line corresponds to $\mu_R^2 = Q^2$, the solid line to the BLM scale setting with $\mu_{\text{min}}^2 = \mu_0^2 = 1$ GeV², while the dash-dotted one denotes the result obtained with the BLM (a) and FAC (b) scale settings. The analogous result for the PMS scale setting is shown as a dotted line. Note that in both panels the BMS DA has been employed and that for the FAC and PMS scale settings N_f has been fixed to 3.

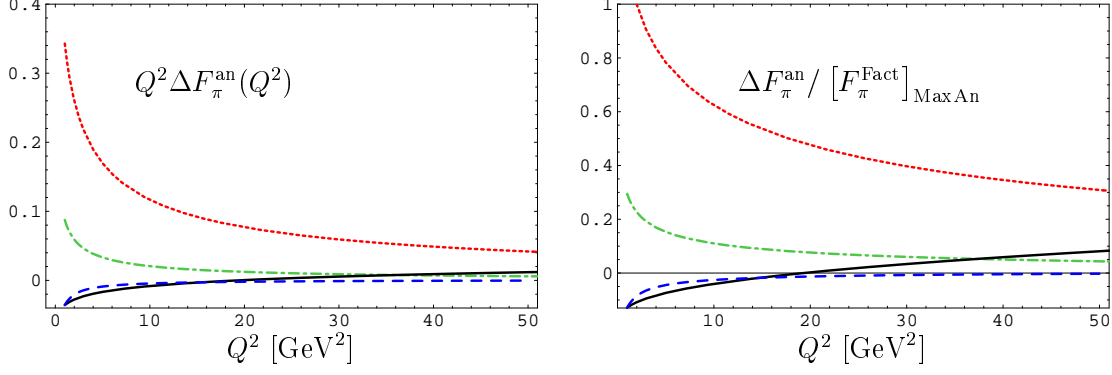


FIG. 10: The NLO analytization ambiguity $Q^2 \Delta F_\pi^{\text{an}}(Q^2)$ (left) and the ratio $\Delta F_\pi^{\text{an}} / [F_\pi^{\text{Fact}}]_{\text{MaxAn}}$ of the NLO analytization ambiguity relative to the factorized pion form factor, computed with the “Maximally Analytic” procedure, (right) within the $\overline{\text{MS}}$ scheme with various scale settings: $\mu_R^2 = Q^2$ (dashed line), BLM (dotted line), BLM (solid line), and the α_V -scheme (dash-dotted line). The curves shown correspond to the BMS DA.

negative and very large below 50 GeV^2 (lying outside the range of Fig. 9(b)) because the corresponding NLO correction is again negative and even larger. The reason for this behavior is that in this scheme the typical parton virtualities in the Feynman diagrams are much lower than the external scale Q^2 (see Table II) giving rise to a large value of the QCD effective coupling.

- The $\overline{\text{BLM}}$ scale setting has two distinct regimes, characterized by the fact that the ratio $R_{\text{NLO}}(Q^2)$ changes its sign around 20 GeV^2 : in the regime below this momentum value, the result for the form factor resembles that found with the $\mu_R^2 = Q^2$ scale setting, though its fall-off with Q^2 is not that steep. On the other hand, above 20 GeV^2 , the form factor almost coincides with the one calculated with the PMS scale setting.

A further complication: it is not clear how to implement quark-mass thresholds when using the FAC and PMS scale settings. Therefore, the predictions shown have been obtained by fixing $N_f = 3$. This is because both scales depend on β_0 and this induces discontinuities in the form factor at the quark-mass thresholds. For that reason, we refrain from using the FAC and PMS schemes in our further considerations. To summarize, all scale settings can be safely used above about 20 GeV^2 , while at smaller Q^2 values, the PMS and FAC settings become unphysical, whereas the $\overline{\text{BLM}}$ and $\mu_R^2 = Q^2$ scale-setting procedures can further be used at values of Q^2 exhausting the validity domain of pQCD. On the other hand, the BLM scale setting remains inapplicable up to scales of the order of 50 GeV^2 (see Fig. 9a). As already explained before, no predictions in the α_V scheme have been shown because this would require the introduction of exogenous IR regulators.

B. Use of non-power series expansions

We turn now to the results obtained in APT. To exploit the effect of the analytization ambiguity on the factorized pion form factor, according to (6.30), we plot in Fig. 10 (left panel)

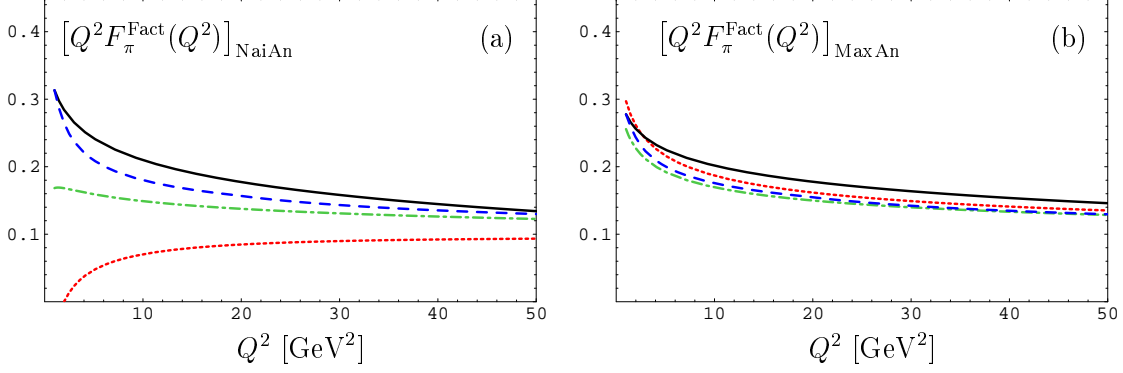


FIG. 11: NLO predictions for $Q^2 F_\pi^{\text{Fact}}$ vs. Q^2 , using the “Naive Analytic” (a) and “Maximally Analytic” (b) procedures and employing the BMS DA. The dashed line corresponds to $\mu_R^2 = Q^2$, the dotted one denotes the result obtained with the standard BLM scale setting, whereas the solid line shows the result calculated with the modified BLM scale setting and the cutoff scale $\mu_0^2 = 1 \text{ GeV}^2$. The results obtained with the α_V -scheme are displayed as a dash-dotted line in both panels.

$$\Delta F_\pi^{\text{an}}(Q^2) = \frac{\mathcal{A}_2^{(2)}(\mu_R^2) - [\bar{\alpha}_s^{(2)}(\mu_R^2)]^2}{\pi} \mathcal{F}_\pi^{\text{NLO}}(Q^2; \mu_R^2) \quad (7.1)$$

and the ratio $\Delta F_\pi^{\text{an}} / [F_\pi^{\text{Fact}}]_{\text{MaxAn}}$ (right panel), employing the BMS DA and the $\overline{\text{MS}}$ scheme with different scale settings. Analogous results for the α_V -scheme are also included; using APT there is no need to introduce external IR regulators.

Summarizing the results in Fig. 10, the main observations are:

- The NLO analytization ambiguity, $\Delta F_\pi^{\text{an}}(Q^2)$, (left panel) and the ratio, $\Delta F_\pi^{\text{an}} / F_\pi^{\text{Fact}}$, (right panel), the latter being computed with the “Maximally Analytic” procedure within the $\overline{\text{MS}}$ scheme with the $\mu_R^2 = Q^2$ (dashed line) and $\overline{\text{BLM}}$ (solid line) scale settings, is small and almost scaling with Q^2 above about 10 GeV^2 , albeit in the second case there is a sign change around 18 GeV^2 . This is because below this momentum, the term $F_\pi^{(1, \text{FG})}$, which is negative, prevails, while above that scale the term $F_\pi^{(1, \beta)}$ becomes dominant due to $-\ln(Q^2/\mu_R^2)$ —in contrast to the former case in which the interplay between these two terms is fixed owing to the absence of the log term. For that reason, the “Maximally Analytic” procedure with the $\overline{\text{BLM}}$ scale setting enhances the form factor at higher Q^2 relative to the “Naive” one.
- The results with the BLM scale setting (dotted line) resemble those computed with the α_V scheme (dash-dotted line). In both cases, $\mathcal{A}_2^{(2)}(\mu_R^2) - [\bar{\alpha}_s^{(2)}(\mu_R^2)]^2$ is large and negative (cf. Fig. 8—right panel), while $\mathcal{F}_\pi^{(1, \text{FG})}$ is also negative. Hence, the overall sign of $\Delta F_\pi^{\text{an}}(Q^2)$ is plus because the $F_\pi^{(1, \beta)}$ is absent. However, in the α_V scheme the shift towards smaller values of the α_s argument is much less pronounced and consequently the enhancement provided by the use of $\mathcal{A}_2^{(2)}(\mu_R^2)$ instead of $[\bar{\alpha}_s^{(2)}(\mu_R^2)]^2$ is rather weak (see also Eq. (5.16)).

Next, we present the results for the factorized pion form factor derived with APT at the NLO level and adopting either the “Naive Analytic” or the “Maximally Analytic” procedure.

From Fig. 11, we see that for both analytization procedures the results for the $\mu_R^2 = Q^2$ (dashed line) and $\overline{\text{BLM}}$ (solid line) scale settings are very close to each other. Note that the α_V -scheme yields a similar result (dash-dotted line), but with a much smaller steepness of the curve at low Q^2 . On the other hand, the standard BLM scale setting (dotted line) produces even an exact cancellation of the NLO and LO terms at the momentum value $Q^2 \approx 2 \text{ GeV}^2$ (so too behaves the ratio $R_{\text{NLO}}(Q^2) = F_{\pi}^{\text{NLO}}(Q^2)/F_{\pi}^{\text{LO}}(Q^2)$ —see Fig. 12(a)). The origin of this cancellation is, however, purely accidental and unphysical: the BLM scale at this point is $\mu_{\text{BLM}}^2 \approx 0.02 \text{ GeV}^2$ with $\alpha_s \approx 0.75$, rendering the pQCD expansion unreliable. This deficiency is lifted when applying the “Maximally Analytic” procedure—see Fig. 11(b). Indeed, such is the impact of the “Maximally Analytic” condition that all renormalization-scheme and scale-setting ambiguities are diminished, with all results for the form factor almost coinciding, as it is obvious from Fig. 11(b). Moreover, from Fig. 11b, we can estimate the effect of varying $\mu_{\text{min}}^2 = \mu_0^2$ in the $\overline{\text{BLM}}$ scale setting procedure by comparing the $\overline{\text{BLM}}$ (black solid) and the BLM (red dotted) curves. Indeed, μ_{BLM}^2 just varies from 0.5 GeV^2 (at $Q^2 = 50 \text{ GeV}^2$) to 0.02 GeV^2 (at $Q^2 = 2 \text{ GeV}^2$), while the difference between these two curves is no more than 10% (using the “Maximally Analytic” condition). Actually, for μ_{min}^2 varying in the range $[1, 0.5] \text{ GeV}^2$, this difference does not even exceed the level of 5%.

Let us close this discussion with some brief comments on the behavior of the ratio $R_{\text{NLO}}(Q^2)$. The message from Fig. 12 is that, except for the BLM scale setting (already discussed), all other scale-settings are not sensitive to the analytization procedure adopted. The induced differences are indeed marginal, with $R_{\text{NLO}}(Q^2)$ being positive, large, and practically scaling with Q^2 for the $\mu_R^2 = Q^2$ scale setting (dashed line), while this quantity in the α_V scheme (dash-dotted line) exhibits the same behavior but with the reverse sign and having approximately half of its magnitude. The situation for the $\overline{\text{BLM}}$ scale setting is somewhat transient between these two options, providing with both analytization procedures enhancement at the low end of Q^2 and reducing the form factor at Q^2 values higher than $Q^2 \simeq 20 \text{ GeV}^2$. This effect is due to the (negative) term $F_{\pi}^{(1,\text{FG})}$ gaining ground against $F_{\pi}^{(1,\beta)}$ that becomes smaller because $\ln(Q^2/\mu_R^2)$ is growing.

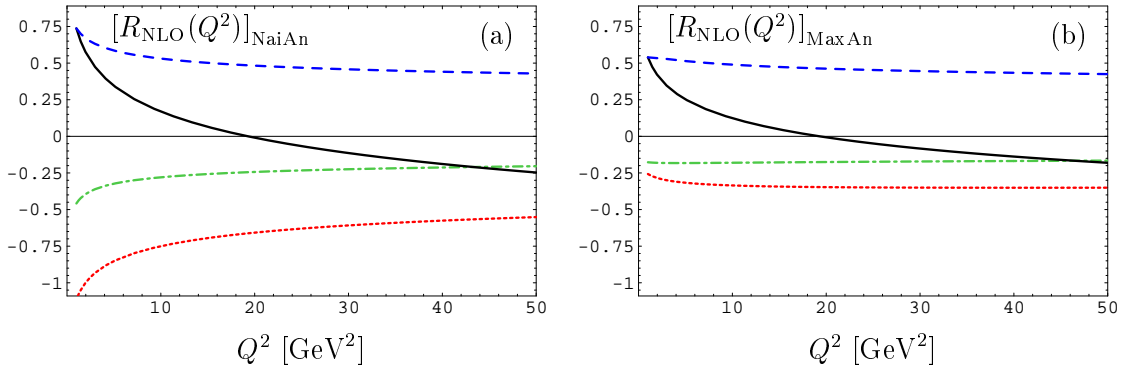


FIG. 12: Results obtained for the ratio $R_{\text{NLO}}(Q^2)$ using the “Naive Analytic” (a) and “Maximally Analytic” (b) procedures and employing the BMS DA. Notations are the same as in figure 11.

C. Non-factorizable Contribution to the Pion Form Factor

So far we have discussed only the factorizable part of the pion form factor (cf. (2.2)). But as argued originally in Refs. [18, 23, 115, 116], and confirmed latter on in several works, for instance, in [21, 25, 28, 29, 79], the dominant contribution at low to moderate values of the momentum transfer $Q^2 \leq 10 \text{ GeV}^2$ originates mainly from the soft contribution that involves no hard-gluon exchanges and is attributed to the Feynman mechanism. At present there is no unique way to calculate this contribution from first principles at the partonic level. One has to resort to theoretical models, based on assumptions that attempt to capture the characteristic features of nonperturbative QCD. In the present investigation we use the Local Duality (LD) approach to calculate the soft contribution, in which it is assumed that the pion form factor is dual to the free quark spectral density [23, 24], i.e.,

$$F_\pi^{\text{LD}}(Q^2) = \frac{1}{\pi^2 f_\pi^2} \int_0^{s_0} \int_0^{s_0} \rho_3(s, s', Q^2) ds ds' = 1 - \frac{1 + 6 s_0/Q^2}{(1 + 4 s_0/Q^2)^{3/2}}, \quad (7.2)$$

with the 3-point spectral density $\rho_3(s, s', t = Q^2)$ given by

$$\rho_3(s, s', t) = \left[t^2 \frac{d^2}{dt^2} + \frac{t^3}{3} \frac{d^3}{dt^3} \right] \frac{1}{\lambda(s, s', t)} \quad (7.3)$$

where

$$\lambda(s, s', t) \equiv \sqrt{(s + s' + t)^2 - 4ss'}. \quad (7.4)$$

Here the duality interval s_0 corresponds to the effective threshold for the higher excited states and the “continuum” in the channels with the axial-current quantum numbers. The LD prescription for the corresponding correlator [22] implies the relation

$$s_0 = 4\pi^2 f_\pi^2. \quad (7.5)$$

A key issue of the soft contribution is the inclusion of Sudakov-type radiative corrections. In [25] only the Sudakov corrections to the quark-photon vertex were taken into account on the basis of [117] leading to a reduction of the soft contribution by approximately 6% at low $Q^2 \simeq 2 \text{ GeV}^2$ and up to 20% at higher Q^2 values. Just recently, however, it was shown in [118] that taking into account all radiative corrections to the correlator, the Sudakov logarithms cancel out. On the face of this finding, we use in this work Eqs. (7.2)–(7.3).

The soft contribution calculated here is consistent with the result obtained in [29] for the asymptotic pion DA on the basis of the soft overlap of the pion wave functions, modelling their k_\perp dependence in terms of the Brodsky–Huang–Lepage Gaussian ansatz [119] and using a constituent-like quark mass of $m_q = 330 \text{ MeV}$. Though the crossover from the soft to the hard regime and the asymptotic behavior are strongly model dependent, with the mass factor $\exp(-\beta_G^2 m_q^2 / x\bar{x})$ (where β_G is the width of the Gaussian distribution, specific for each particular pion DA) playing an important role in tuning this behavior—see [21] for a detailed analysis—the trend at lower values of Q^2 up to about 4 GeV^2 is approximately the same. Similar results were also obtained in [120] using a Bethe-Salpeter equation and a constituent-type quark mass of $m_q = 330 \text{ MeV}$. In both approaches mentioned [29, 120] the quark mass in the hard part was set equal to zero and the effective QCD coupling was assumed to saturate at low Q^2 with a transition scale from soft to hard in the range $Q^2 \simeq 12 - 18 \text{ GeV}^2$.

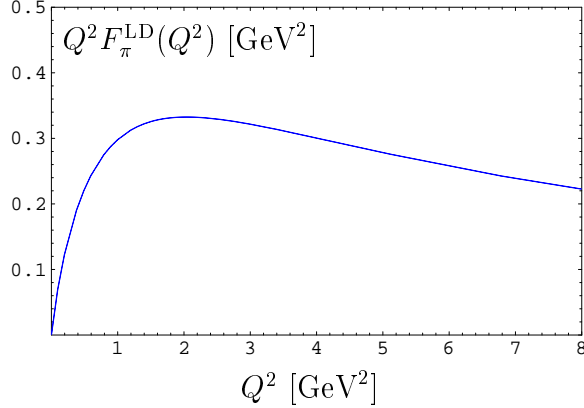


FIG. 13: Calculation of the soft part of the pion form factor in the Local Duality approach.

D. Comparison with experimental data

It is time to step up one level higher and consider the total form factor in order to compare our theoretical predictions with the experimental data. So far we have considered the factorized hard contribution to the pion form factor only at higher values of Q^2 , where pQCD is safe. However, attempting to compute the total pion form factor in the full Q^2 range, according to Eq. (2.2), we have to combine this contribution with the soft part. Recall that we have neglected in the hard-scattering amplitude (i.e., in the parton propagators—cf. Eqs. (A1), (A6a), and (A7)) all parton transverse momenta against the large scale Q^2 and integrated out in the pion wave functions all transverse momenta up to the scale μ_0^2 . But below some momentum scale of this order, these contributions in T_H start to be comparable (especially in the endpoint region where $x \rightarrow 1$) and, a fortiori, the collinear factorization becomes increasingly unreliable. To avoid this happening, we have to restrict the evaluation of the hard form-factor contribution to that Q^2 domain compatible with the collinear approximation. In technical terms this means that below the scale s_0 (the duality threshold) we have to switch from the parton representation to the hadron representation according to local duality.⁸

As we have seen in Sec. V, fixing the renormalization scale μ_R^2 in all considered schemes entails problems related to the small Q^2 -behavior of the factorizable term of the pion form factor: the NLO-term can reach the level of 50% of the LO part, casting doubts on the validity of the perturbative expansion per se. In addition, both terms (LO and NLO) generate a fast growth of the form factor at small Q^2 , artificially induced by large values of the strong coupling and by a $1/Q^2$ -factor. The origin of this failure, as stated above, can be traced to the violation of the collinear factorization approximation, i.e., the resurrection of small momenta in T_H that have initially been neglected and absorbed into the pion DA.⁹

Hence, it becomes clear that we must correct the factorization results in the low- Q^2 region

⁸ A smooth transition from the partonic to the hadronic regime may go via an intermediate constituent-quark formation due to QCD dressing. Because there is no unambiguous way to do this, we prefer to ignore this regime here (and refer for a discussion of such dressed quarks to [29]).

⁹ Their explicit inclusion would give logarithmic and power-behaved corrections amounting to Sudakov-type exponentials containing perturbative [88] and nonperturbative corrections [60].

in order to ensure that each contribution lies in the corresponding domain of validity. To achieve this goal, we need a conceptual framework.

This is provided by gauge invariance that protects the value of $F_\pi(0)$ by means of the Ward identity relating a three-point Feynman diagram at zero-momentum transfer to a 2-point diagram. Consider the L -loop approximation in the LD approach. Then, using the replacements $s_0 \rightarrow s_0^{L\text{-loop}}$ and $\rho_3(s, s', Q^2; \mu_R^2) \rightarrow \rho_3^{L\text{-loop}}(s, s', Q^2; \mu_R^2)$, Eq. (7.2) relates $F_\pi^{\text{LD}}(Q^2)$ to the integrated 3-point spectral density $\rho_3^{L\text{-loop}}(s, s', Q^2; \mu_R^2)$, which is now dependent on μ_R^2 . Recall that the Ward identity links the 2-point (i.e., axial-axial current) spectral density $\rho_2^{L\text{-loop}}(s; \mu_R^2)$ to the 3-point (vector-axial-axial current) spectral density $\rho_3^{L\text{-loop}}(s, s', 0; \mu_R^2)$ in the following way

$$\rho_3^{L\text{-loop}}(s, s', 0; \mu_R^2) = \pi \delta(s - s') \rho_2^{L\text{-loop}}(s; \mu_R^2). \quad (7.6)$$

Taking into account the LD expression for the pion decay constant,

$$f_\pi^2 = \frac{1}{\pi} \int_0^{s_0^{L\text{-loop}}} \rho_2^{L\text{-loop}}(s; \mu_R^2) ds, \quad (7.7)$$

one finds

$$F_\pi^{\text{LD}}(0; \mu_R^2) = 1. \quad (7.8)$$

The 2-loop approximation for the spectral density, $\rho_2^{2\text{-loop}}(s; \mu_R^2)$, can be obtained from the e^+e^- cross-section $R(s)$ [121], because these quantities in massless QCD are proportional to each other, so that

$$\rho_2^{2\text{-loop}}(s; \mu_R^2) = \frac{1}{4\pi} \left[1 + \frac{\alpha_s(\mu_R^2)}{\pi} + \left(\frac{\alpha_s(\mu_R^2)}{\pi} \right)^2 \left(r_2 - \frac{b_0}{4} \ln \frac{s}{\mu_R^2} \right) \right]; \quad (7.9)$$

$$r_2 = \frac{3}{4} C_F \left[\frac{1}{12} C_A - \frac{1}{8} C_F + b_0 \left(\frac{11}{8} - \zeta(3) \right) \right], \quad (7.10)$$

where $\zeta(3)$ is the Riemann Zeta function. Then, Eq. (7.7) yields the following nonlinear relation for the 2-loop effective threshold $s_0^{2\text{-loop}}$

$$s_0^{2\text{-loop}} \left\{ 1 + \frac{\alpha_s(\mu_R^2)}{\pi} + \left(\frac{\alpha_s(\mu_R^2)}{\pi} \right)^2 \left[r_2 - \frac{b_0}{4} \left(\ln \frac{s_0^{2\text{-loop}}}{\mu_R^2} - 1 \right) \right] \right\} = 4\pi^2 f_\pi^2 \quad (7.11)$$

that replaces the standard LD relation, notably, Eq. (7.5). Note in this context that the effective 2-loop threshold $s_0^{2\text{-loop}}$ should be used only in formulas containing the 2-loop spectral density $\rho_3^{2\text{-loop}}(s, s', Q^2)$. Were we in the position to write down the 2-loop spectral density $\rho_3^{2\text{-loop}}(s, s', Q^2)$ for all Q^2 values, then we would have obtained via Eqs. (7.2)-(7.7) an expression for the pion form factor valid at $O(\alpha_s^2)$. Instead, we use the leading-order LD expression, $F_\pi^{\text{LD}}(Q^2; \mu_R^2)$, and add perturbative $O(\alpha_s)$ - and $O(\alpha_s^2)$ -corrections explicitly in terms of $F_\pi^{\text{Fact}}(Q^2; \mu_R^2)$. Recalling Eq. (7.8), we then have

$$F_\pi^{\text{Fact}}(Q^2 = 0; \mu_R^2) = 0. \quad (7.12)$$

The next task is to match this low- Q^2 value with the large- Q^2 result of pQCD, $F_\pi^{\text{Fact}}(Q^2; \mu_R^2)$. The most straightforward way is to adopt $F_\pi^{\text{Fact}}(Q^2; \mu_R^2)$ at large Q^2 and correct its singular

($\sim 1/Q^2$) behavior at small Q^2 by introducing some reasonable mass scale M_0^{-1} via the replacement¹⁰

$$F_\pi^{\text{Fact}}(Q^2; \mu_R^2) \equiv \tilde{F}_\pi(Q^2; \mu_R^2) \frac{M_0^2}{Q^2} \rightarrow \tilde{F}_\pi(Q^2; \mu_R^2) \frac{M_0^2}{M_0^2 + Q^2}. \quad (7.13)$$

However, this expression has the wrong limit at $Q^2 = 0$, so that one needs to correct it in order to maintain the Ward identity (WI):

$$F_\pi^{\text{Fact-WI}}(Q^2; \mu_R^2) = -\tilde{F}_\pi(Q^2; \mu_R^2) \Phi(Q^2/M_0^2) + \tilde{F}_\pi(Q^2; \mu_R^2) \frac{M_0^2}{M_0^2 + Q^2}. \quad (7.14)$$

Here the function $\Phi(z)$ is some smooth function with $\Phi(0) = 1$ and $z\Phi(z) \rightarrow 0$ when $z \rightarrow \infty$, introduced to preserve the high Q^2 -asymptotics of $F_\pi^{\text{Fact}}(Q^2; \mu_R^2)$. The simplest choice for $\Phi(z)$ is $\Phi(z) = 1/(1+z)^2$, yielding

$$\begin{aligned} F_\pi^{\text{Fact-WI}}(Q^2; \mu_R^2) &= \tilde{F}_\pi(Q^2; \mu_R^2) \frac{M_0^2}{M_0^2 + Q^2} \left(1 - \frac{M_0^2}{M_0^2 + Q^2} \right) \\ &= F_\pi^{\text{Fact}}(Q^2; \mu_R^2) \left(\frac{Q^2}{M_0^2 + Q^2} \right)^2. \end{aligned} \quad (7.15)$$

The scale parameter M_0^2 should be identified with the threshold $2s_0^{2\text{-loop}}$ to read $M_0^2 = 2s_0^{2\text{-loop}}$ because $s_0^{2\text{-loop}}$ is the “natural” scale parameter for the 2-point correlator in the pion case, while the scale characterizing the 3-point correlator, corresponding to the form factor, is two times larger [67].

In this way, we finally arrive at

$$F_\pi^{\text{Fact-WI}}(Q^2; \mu_R^2) = \left(\frac{Q^2}{2s_0^{2\text{-loop}} + Q^2} \right)^2 F_\pi^{\text{Fact}}(Q^2; \mu_R^2). \quad (7.16)$$

We are now in the position to supply an expression for the total pion form factor valid in the whole Q^2 range:

$$F_\pi(Q^2; \mu_R^2) = F_\pi^{\text{LD}}(Q^2) + F_\pi^{\text{Fact-WI}}(Q^2; \mu_R^2). \quad (7.17)$$

This expression comprises the NLO prediction for the factorized part under the proviso of the Ward identity at $Q^2 = 0$ and the non-factorizable soft part. [Parenthetically, note the explicit μ_R^2 dependence of this expression as a consequence of the truncation of the perturbative series (see Eqs. (4.1)–(4.8)).]

Before continuing with the presentation of our final results, let us remark that a similar type of matching has been applied by Radyushkin [24] to describe the pion form factor, providing the result

$$F_\pi(Q^2) = \frac{F_\pi^{\text{LD}(0)}(Q^2) + (\alpha_s/\pi) [1 + Q^2/(2s_0)]^{-1}}{1 + \alpha_s/\pi} \quad (7.18)$$

¹⁰ One may think of this scale as corresponding to the maximum transverse quark antiquark separation $b_0 \sim M_0$ still accessible to the hard form factor via hard-gluon exchange just before the crossover to the nonperturbative dynamics.

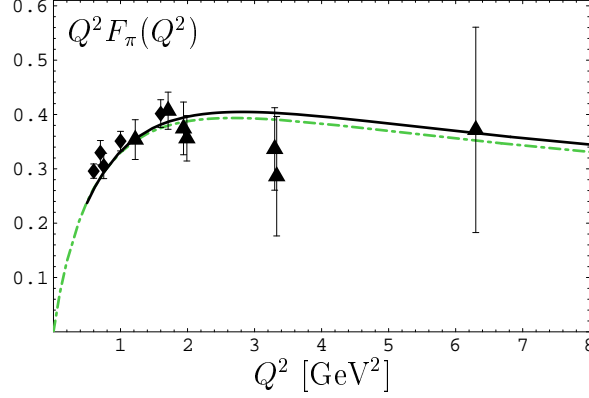


FIG. 14: Comparison of the pion form factor calculated by Radyushkin [24] using the LD approach and interpolation from low to high Q^2 (dash-dotted line) with our result for the total form factor given by Eq. (7.17), computed with the asymptotic DA in the $\overline{\text{MS}}$ scheme with the $\overline{\text{BLM}}$ scale setting and using LO APT (solid line). The experimental data are taken from [36] (diamonds) and [122], [123] (triangles).

illustrated in Fig. 14 (a) (dash-dotted line). In this equation—which follows the Brodsky–Lepage interpolation formula for the $\pi\gamma$ -transition form factor [124]—the first term means the soft form factor calculated with the LD approach, while the second one includes the LO radiative corrections. It is evident from this figure that Radyushkin’s result is very close to that given by Eq. (7.17), evaluated with the asymptotic DA in the $\overline{\text{MS}}$ scheme with the $\overline{\text{BLM}}$ scale setting using for the sake of comparison LO APT (solid line).

Employing the above considerations we now present predictions for the total scaled form factor vs. Q^2 in different renormalization schemes and perturbation-theory approaches using the BMS pion DA. Figure 15 shows the results for the standard perturbation theory within the $\overline{\text{MS}}$ scheme adopting the $\mu_R^2 = Q^2$ (dashed line) and the $\overline{\text{BLM}}$ (solid line) scale settings. In Fig. 16 we present analogous predictions calculated with the APT. In this case, it is possible to include results computed with the BLM scale setting and to use the α_V scheme. We observe from this figure (left panel) that the “Naive Analytization” gives results that bear a rather strong scheme and scale-setting dependence. In contrast, applying the “Maximal Analytic” procedure, the arbitrariness in the scheme and scale setting is minimized—Fig. 16(b) being a graphic proof of that. Note that this figure shows also separately the soft part of the form factor, displayed in Fig. 13, and the hard contributions corresponding to the various scheme and scale settings discussed above and presented in Fig. 11(b).

The phenomenological upshot of our analysis is summarized in the left panel of Fig. 17, where we show predictions for the whole BMS “bunch” of pion DAs [1]. The shaded strip incorporates the nonperturbative uncertainties related to non local QCD sum rules and also the ambiguities induced by the scheme and renormalization scale setting—in correspondence to Fig. 16. Note that the two broken lines mark the region of predictions associated with the asymptotic pion DA. These results can be compared with previous theoretical predictions and also with further experimental data to be obtained at JLab (see right part of Fig. 17, taken from [37]). The data points extending to Q^2 of 6 GeV^2 are expectations from projected experiments at JLab after the planned upgrade of CEBAF to 12 GeV (we refer to [37] for further explanations and related references).

These striking findings give convincing evidence that the end-point suppressed structure of the BMS type pion DA not only provides best agreement with the CLEO and CELLO

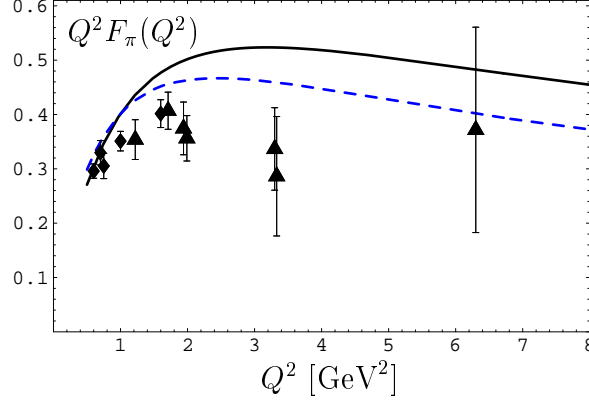


FIG. 15: Theoretical predictions for $Q^2 F_\pi(Q^2)$ obtained with the BMS pion DA using standard pQCD within the $\overline{\text{MS}}$ scheme and adopting the $\mu_R^2 = Q^2$ (dashed line) and BLM (solid line) scale settings. The experimental data are taken from [36] (diamonds) and [122], [123] (triangles).

data (cf. Fig. 4), it also allows to describe the pion form-factor data with at least the same quality as with the asymptotic pion DA—as it becomes evident from the LHS of Fig. 17.

VIII. SUMMARY AND CONCLUSIONS

In summary, the key concepts and merits arising from this analysis are as follows.

- We worked out interpolation formulas for the analytic coupling constant and its analytic second power that take into account heavy-flavor thresholds and greatly facilitate calculations. This allowed us to develop a theoretical procedure and apply its numer-

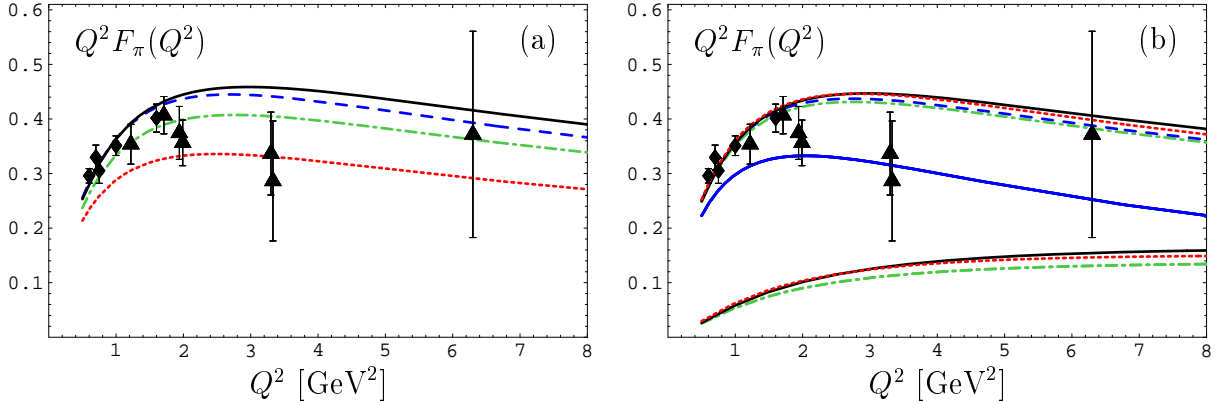


FIG. 16: Theoretical predictions for $Q^2 F_\pi(Q^2)$ using analytic perturbation theory and the BMS DA in conjunction with the “Naive Analytic” (a) and “Maximally Analytic” (b) analytization procedures. Different scale settings within the $\overline{\text{MS}}$ scheme are used: $\mu_R^2 = Q^2$ (dashed line), BLM (dotted line), and BLM (solid line). The dash-dotted line represents the prediction obtained with the α_V -scheme. Also included are the prediction for the soft form-factor part (solid blue line) and below this, the hard contributions in correspondence with the predictions for the total form factor on the upper part of the figure. The experimental data are taken from [36] (diamonds) and [122], [123] (triangles).

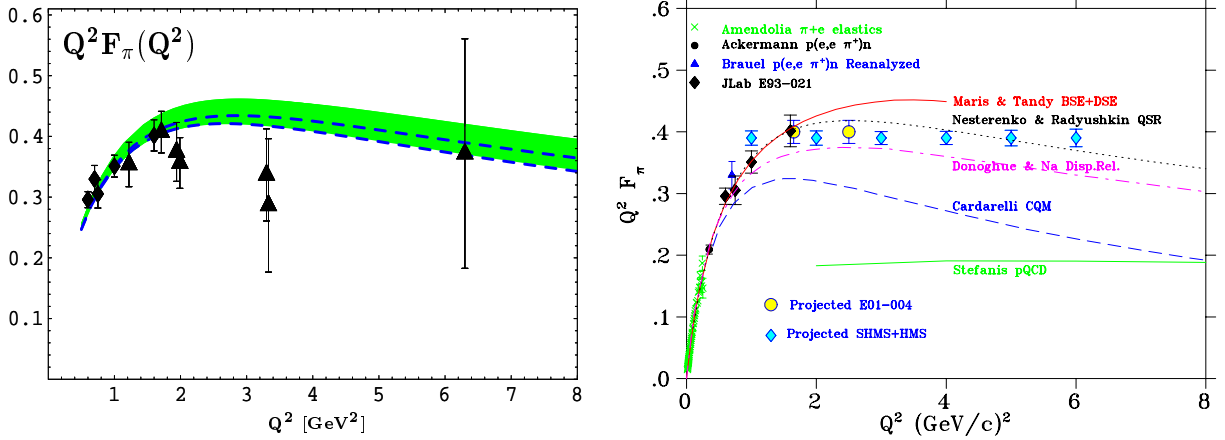


FIG. 17: (Left) Predictions for the scaled pion form factor calculated with the BMS bunch (green strip) encompassing nonperturbative uncertainties from nonlocal QCD sum rules [1] and renormalization scheme and scale ambiguities at the level of the NLO accuracy, as discussed in Fig. 16. The dashed lines inside the strip indicate the corresponding area of predictions obtained with the asymptotic pion DA. Note that this strip contains only perturbative scheme and scale ambiguities at the level of the NLO accuracy, calculated in APT with the “Maximally Analytic” procedure. The experimental data are taken from [36] (diamonds) and [122], [123] (triangles). (Right) Summary of existing and projected experimental data on the electromagnetic pion form factor in comparison with the results of various theoretical calculations; figure taken from [37] (see there for explanations).

ical realization in order to compute the evolution of the pion DA using NLO analytic perturbation theory. The hard form factor was corrected at low Q^2 as to fulfill the Ward identity and was added to the soft form factor, derived via Local Duality, without introducing double counting.

- On the theoretical front, we found that replacing the QCD effective coupling and its powers by their analytic images—a procedure we termed “Maximally Analytic”—not only provides IR protection to the coupling, it also helps diminishing the renormalization scheme and scale-setting dependence of the form-factor predictions already at the NLO level, rendering the calculation of still higher-order corrections virtually superfluous.
- From the phenomenological point of view, our most discernible result is that the BMS pion DA [1] (out of a “bunch” of similar doubly-peaked endpoint-suppressed pion DAs) yields to predictions for the electromagnetic form factor very close to those obtained with the asymptotic pion DA. Hence, concerns that a double-humped pion DA could jeopardize the sound application of pQCD are unduly. Conversely, we have shown that a small deviation of the prediction for the pion form factor from that obtained with the asymptotic pion DA does not necessarily imply that the underlying pion DA has to be close to the asymptotic profile. Much more important is the behavior of the pion DA in the endpoint region $x \rightarrow 0, 1$.

Looking further into the future is yet more exciting. With the planned upgrade of the CEBAF experiment to 12 GeV, the pion’s electromagnetic form factor can be studied up

to $Q^2 \simeq 6 \text{ GeV}^2$ [37], providing crucial constraints to verify the various theoretical predictions discussed here and elsewhere. The apparently good agreement of our results with the available experimental data (see Fig. 17) is encouraging.

Acknowledgments

We wish to thank Blaženka Melić, Sergey Mikhailov, Dieter Müller, Dan Pirjol, Dmitry Shirkov and Igor Solovtsov for useful discussions, and Badri Magradze for supplying us with unpublished numerical data on $\bar{\alpha}_s^{(2)}(Q^2)$ and $\mathcal{A}_2^{(2)}(Q^2)$ that take into account quark mass thresholds. We would also like to thank Henk Blok and Garth Huber for providing information on the current pion form-factor experimental data. Two of us (A.P.B. and K.P.-K.) are indebted to Prof. Klaus Goeke for the warm hospitality at Bochum University, where the major part of this investigation was carried out. This work was supported in part by the Deutsche Forschungsgemeinschaft (Projects 436 KRO 113/6/0-1 and 436 RUS 113/752/0-1), the Heisenberg–Landau Programme (grants 2002 and 2003), the COSY Forschungsprojekt Jülich/Bochum, the Russian Foundation for Fundamental Research (grants No. 03-02-16816 and 03-02-04022), the INTAS-CALL 2000 N 587, and by the Ministry of Science and Technology of the Republic of Croatia under Contract No. 0098002. The work of W.S. was supported in part by a Feodor-Lynen Fellowship from the Alexander von Humboldt Foundation and in part by the U.S. Department of Energy (D.O.E.) under cooperative research agreement #DF-FC02-94ER40818.

APPENDIX A: HARD-SCATTERING AMPLITUDE FOR THE PION'S ELECTROMAGNETIC FORM FACTOR AT NLO

In this section we list the NLO results for the hard-scattering amplitude [26, 80, 81, 82, 83, 84, 85], used in our analysis.

The LO contribution to $T_H(x, y, Q^2; \mu_F^2)$, expanded as in (2.4), reads

$$T_H^{(0)}(x, y, Q^2) = \frac{N_T}{Q^2} \frac{1}{\bar{x}\bar{y}}, \quad (\text{A1})$$

where

$$N_T = \frac{2\pi C_F}{C_A} = \frac{8\pi}{9}, \quad (\text{A2})$$

$C_F = (N_c^2 - 1)/2N_c = 4/3$, $C_A = N_c = 3$ are the color factors of $SU(3)_c$, and the notation $\bar{z} \equiv 1 - z$ has been used. The usual color decomposition of the NLO correction—marked by self-explainable labels—is given by

$$T_H^{(1)}(Q^2; \mu_F^2, \mu_R^2) = C_F T_H^{(1,F)}(Q^2; \mu_F^2) + b_0 T_H^{(1,\beta)}(Q^2; \mu_R^2) + C_G T_H^{(1,G)}(Q^2), \quad (\text{A3})$$

where $C_G = (C_F - C_A/2)$ and the first coefficients of the β function are

$$b_0 = \frac{11}{3}C_A - \frac{4}{3}T_R N_f, \quad b_1 = \frac{34}{3}C_A^2 - \left(4C_F + \frac{20}{3}C_A\right) T_R N_f. \quad (\text{A4})$$

Here, $T_R = 1/2$ and N_f denotes the number of flavors, whereas the expansion of the β -function in the NLO approximation is given by

$$\beta(\alpha_s(\mu^2)) = -\alpha_s(\mu^2) \left\{ b_0 \left[\frac{\alpha_s(\mu^2)}{4\pi} \right] + b_1 \left[\frac{\alpha_s(\mu^2)}{4\pi} \right]^2 \right\}. \quad (\text{A5})$$

With reference to the application of the BLM [62] scale setting in fixing the renormalization point, we single out the b_0 -proportional (i.e., N_f -dependent) term, given by

$$T_H^{(1,\beta)}(x, y, Q^2; \mu_R^2) = \frac{N_T}{Q^2} \frac{1}{\bar{x}\bar{y}} \left[\frac{5}{3} - \ln(\bar{x}\bar{y}) - \ln \frac{Q^2}{\mu_R^2} \right], \quad (\text{A6a})$$

and present the remainder of T_H as a color decomposition in the form

$$\begin{aligned} T_H^{(1,F)}(x, y, Q^2; \mu_F^2) = & \frac{N_T}{Q^2} \frac{1}{\bar{x}\bar{y}} \left[-\frac{28}{3} + \left(6 - \frac{1}{x}\right) \ln \bar{x} + \left(6 - \frac{1}{y}\right) \ln \bar{y} + \ln^2(\bar{x}\bar{y}) \right. \\ & \left. + 2 \ln \frac{Q^2}{\mu_F^2} (3 + \ln(\bar{x}\bar{y})) \right] \end{aligned} \quad (\text{A6b})$$

$$\begin{aligned} T_H^{(1,G)}(x, y, Q^2) = & \frac{N_T}{Q^2} \frac{1}{\bar{x}\bar{y}} \left[-\frac{20}{3} - 8 \frac{\ln \bar{x}}{x} - 8 \frac{\ln \bar{y}}{y} - 2 \ln \bar{x} \ln \bar{y} - 2 \ln x \ln y \right. \\ & \left. + 2 \ln x \ln \bar{y} + 2 \ln \bar{x} \ln y - 2(1 - x - y)H(x, y) - 2R(x, y) \right] \end{aligned} \quad (\text{A6c})$$

for the color singlet and color non-singlet parts, respectively. For calculational convenience, we also supply the sum of these terms (cf. Eq. (4.7)):

$$\begin{aligned}
T_{\text{H}}^{(1,\text{FG})}(x, y, Q^2; \mu_{\text{F}}^2) &= C_{\text{F}} T_{\text{H}}^{(1,\text{F})}(x, y, Q^2; \mu_{\text{F}}^2) + C_{\text{G}} T_{\text{H}}^{(1,\text{G})}(x, y, Q^2) \\
&= \frac{N_{\text{T}}}{Q^2} \frac{1}{\bar{x}\bar{y}} \frac{1}{3} \left\{ -34 + 24 \ln(\bar{x}\bar{y}) + 4 \ln^2(\bar{x}\bar{y}) \right. \\
&\quad + \ln x \ln y + \ln \bar{x} \ln \bar{y} - \ln x \ln \bar{y} - \ln \bar{x} \ln y \\
&\quad \left. + (1-x-y) \text{H}(x, y) + \text{R}(x, y) + 8 [3 + \ln(\bar{x}\bar{y})] \ln \frac{Q^2}{\mu_{\text{F}}^2} \right\}, \quad (\text{A7})
\end{aligned}$$

where

$$\begin{aligned}
\text{H}(x, y) &= \frac{1}{1-x-y} \left[\text{Li}_2\left(\frac{\bar{y}}{x}\right) + \text{Li}_2\left(\frac{\bar{x}}{y}\right) + \text{Li}_2\left(\frac{xy}{\bar{x}\bar{y}}\right) \right. \\
&\quad \left. - \text{Li}_2\left(\frac{x}{\bar{y}}\right) - \text{Li}_2\left(\frac{y}{\bar{x}}\right) - \text{Li}_2\left(\frac{\bar{x}\bar{y}}{xy}\right) \right] \quad (\text{A8a})
\end{aligned}$$

with Li_2 being the di-logarithm function, defined by $\text{Li}_2(z) = -\int_0^z \frac{\ln(1-t)dt}{t}$, and

$$\begin{aligned}
\text{R}(x, y) &= \frac{1}{(x-y)^2} \left[(2xy - x - y)(\ln x + \ln y) \right. \\
&\quad + (-2xy^2 - 2y^2 + 10xy - 2y - 4x^2) \frac{\ln \bar{y}}{y} \\
&\quad + (-2yx^2 - 2x^2 + 10xy - 2x - 4y^2) \frac{\ln \bar{x}}{x} \\
&\quad \left. - (y\bar{y}^2 + x\bar{x}^2) \text{H}(x, \bar{y}) \right]. \quad (\text{A8b})
\end{aligned}$$

APPENDIX B: FACTORIZATION SCALE DEPENDENCE IN STANDARD PQCD

Here we examine the μ_{F}^2 -dependence of the hard-scattering amplitude (see, for example, [9, 11, 27, 77, 125]). We start with the representation for $T_{\text{H}}(\mu_{\text{F}}^2, \mu_{\text{R}}^2)$, given by (2.4), to get

$$T_{\text{H}}(\mu_{\text{F}}^2, \mu_{\text{R}}^2) = \alpha_s(\mu_{\text{R}}^2) \left[T_{\text{H}}^{(0)} + \frac{\alpha_s(\mu_{\text{R}}^2)}{4\pi} T_{\text{H}}^{(1)}(\mu_{\text{F}}^2, \mu_{\text{R}}^2) \right] \quad (\text{B1})$$

with $T_{\text{H}}^{(0)}(x, y, Q^2)$ and $T_{\text{H}}^{(1)}(x, y, Q^2; \mu_{\text{F}}^2, \mu_{\text{R}}^2)$ as in (A1) and (A3) for the LO and NLO, respectively. These functions can be represented as follows

$$T_{\text{H}}^{(0)} = N_{\text{T}} C_0(x, y, Q^2), \quad \text{and} \quad C_0 = \frac{1}{\bar{x}\bar{y}Q^2}, \quad (\text{B2})$$

$$\begin{aligned}
T_{\text{H}}^{(1)}(\mu_{\text{F}}^2, \mu_{\text{R}}^2) &= \ln\left(\frac{Q^2}{\mu_{\text{F}}^2}\right) \left[T_{\text{H}}^{(0)}(x, s, Q^2) \otimes_s V_0(s, y) + V_0(s, x) \otimes_s T_{\text{H}}^{(0)}(s, y, Q^2) \right] \\
&\quad - b_0 \ln\left(\frac{Q^2}{\mu_{\text{R}}^2}\right) T_{\text{H}}^{(0)}(x, y, Q^2) + N_{\text{T}} C_1(x, y, Q^2), \quad (\text{B3})
\end{aligned}$$

where $C_1(x, y, Q^2)$ absorbs all other μ_F^2 - and μ_R^2 -independent terms from (A3). Using this structure with respect to the μ_F^2 -dependence, we can conclude that

$$\frac{dT_H}{d \ln \mu_F^2} = -T_H(\mu_F^2, \mu_R^2) \otimes V(\alpha_s(\mu_R^2)) - V(\alpha_s(\mu_R^2)) \otimes T_H(\mu_F^2, \mu_R^2) + O(\alpha_s^3), \quad (\text{B4})$$

where $V(\alpha_s(\mu_R^2))$ is the ERBL evolution kernel (C2). Then, the whole derivative of the form factor (2.3) is

$$\begin{aligned} \frac{dF_\pi(Q^2; \mu_R^2)}{d \ln \mu_F^2} &= \Phi_\pi(\mu_F^2) \otimes T_H(\mu_F^2, \mu_R^2) \otimes [V(\alpha_s(\mu_F^2)) - V(\alpha_s(\mu_R^2))] \otimes \Phi_\pi(\mu_F^2) \\ &+ \Phi_\pi(\mu_F^2) \otimes [V(\alpha_s(\mu_F^2)) - V(\alpha_s(\mu_R^2))] \otimes T_H(\mu_F^2, \mu_R^2) \otimes \Phi_\pi(\mu_F^2) \\ &+ O(\alpha_s^3). \end{aligned} \quad (\text{B5})$$

Recalling that in the 2-loop approximation of the standard pQCD

$$\frac{d\alpha_s(\mu^2)}{d \ln \mu^2} = -4\pi b_0 \left[\frac{\alpha_s(\mu^2)}{4\pi} \right]^2 [1 + O(\alpha_s(\mu^2))], \quad (\text{B6})$$

we have

$$V(\alpha_s(\mu_F^2)) - V(\alpha_s(\mu_R^2)) = \left[\frac{\alpha_s(\mu_F^2) - \alpha_s(\mu_R^2)}{4\pi} \right] V_0 + O(\alpha_s^2) = O(\alpha_s^2), \quad (\text{B7})$$

so that

$$\frac{dF_\pi(Q^2; \mu_R^2)}{d \ln \mu_F^2} = O(\alpha_s^3). \quad (\text{B8})$$

Hence, we conclude that at the level of the NLO approximation of the standard pQCD, the violation of the factorization-scale independence is one order of α_s higher.¹¹

APPENDIX C: TWO-LOOP EVOLUTION OF THE PION DISTRIBUTION AMPLITUDE IN STANDARD PQCD

The pion distribution amplitude $\varphi_\pi(x, \mu_F^2)$ satisfies an evolution equation of the form

$$\frac{d\varphi_\pi(x, \mu_F^2)}{d \ln \mu_F^2} = V(x, u, \alpha_s(\mu_F^2)) \otimes_u \varphi_\pi(u, \mu_F^2), \quad (\text{C1})$$

where $V(x, u, \alpha_s(\mu_F^2))$ is the perturbatively calculable NLO evolution kernel

$$V(x, u, \alpha_s) = \frac{\alpha_s}{4\pi} V_0(x, u) + \frac{\alpha_s^2}{(4\pi)^2} V_1(x, u). \quad (\text{C2})$$

¹¹ Moreover, the dependence on μ_F^2 of the NLO prediction for the pion form factor was investigated in [26], where it was found that these results vary only slightly with μ_F^2 rendering the “factorization-scheme ambiguity” to be small.

If the distribution amplitude $\varphi_\pi(x, \mu_0^2)$ is determined at an initial momentum scale μ_0^2 (using some nonperturbative methods), then the integro-differential evolution equation (C1) can be integrated using the moment method to give $\varphi_\pi(x, \mu_F^2)$ at any momentum scale μ_F^2 . The one-[12] and two-loop [126, 127, 128] corrections to the evolution kernel were determined in the $\overline{\text{MS}}$ -scheme, but because of the complicated structure of the two-loop corrections, only the numerical evaluation of the (first few) moments of the evolution kernel was possible [129, 130]. However, making use of conformal-symmetry constraints, the complete analytical form of the NLO solution of the evolution equation (C1) has been obtained [70, 71]. We note that for $\mu_F^2 \rightarrow \infty$ the solution of Eq. (C1) takes the asymptotic form $\varphi_\pi(x, \mu_F^2 \rightarrow \infty) \equiv \varphi_{\text{as}}(x) = 6x(1-x)$.

The pion DA can be cast in the form

$$\varphi_\pi(x, \mu_F^2) = U(x, s; \mu_F^2, \mu_0^2) \otimes_s \varphi_\pi(s, \mu_0^2), \quad (\text{C3})$$

where the operator $U(x, s; \mu_F^2, \mu_0^2)$ describes the evolution from the scale μ_0^2 to the scale μ_F^2 and represents the solution of an evolution equation equivalent to (C1), given by

$$\frac{d}{d \ln \mu_F^2} U(x, s; \mu_F^2, \mu_0^2) = V(x, u, \alpha_s(\mu_F^2)) \otimes_u U(u, s; \mu_F^2, \mu_0^2). \quad (\text{C4})$$

It is convenient to express the nonperturbative input DA, $\varphi_\pi(x, \mu_0^2)$, as an expansion over Gegenbauer polynomials $C_k^{3/2}(2x-1)$ which represent the eigenfunctions of the LO kernel V_0 , i.e.,

$$\varphi_\pi(x, \mu_0^2) = 6x(1-x) \left[1 + \sum_{m=2}^{\infty} 'a_m(\mu_0^2) C_m^{3/2}(2x-1) \right], \quad (\text{C5})$$

in which \sum' denotes the sum over even indices only. The nonperturbative input is now contained in the $a_m(\mu_0^2)$ coefficients. The Gegenbauer polynomials $C_n^{3/2}(2x-1)$ satisfy the orthogonalization condition

$$\int_0^1 dx x(1-x) C_n^{3/2}(2x-1) C_m^{3/2}(2x-1) = N_n \delta_{nm} \quad (\text{C6})$$

with respect to the weight $x(1-x)$, where

$$N_n = \frac{(n+1)(n+2)}{4(2n+3)}. \quad (\text{C7})$$

The moments of the evolution kernel

$$M_{kn} [\alpha_s(\mu_F^2)] = C_k^{3/2}(2x-1) \otimes_x V(x, y; \alpha_s(\mu_F^2)) \otimes_y \frac{y(1-y)}{N_n} C_n^{3/2}(2y-1), \quad (\text{C8a})$$

or, equivalently, the anomalous dimensions

$$\gamma_{kn} [\alpha_s(\mu_F^2)] = -2M_{kn} [\alpha_s(\mu_F^2)], \quad (\text{C8b})$$

represent the elements of the triangular matrix ($k \geq n$). While the LO kernel is diagonal with respect to the Gegenbauer polynomials $C_n^{3/2}$ (only the $\gamma_{nn}^{(0)} \equiv \gamma_n^{(0)}$ elements appear), the

structure of the NLO and still higher-order kernels leads to the appearance of off-diagonal terms in the matrix of the anomalous dimensions (both types of terms $\gamma_{nn}^{(1)} \equiv \gamma_n^{(1)}$ as well as $\gamma_{kn}^{(1)}$, $k > n$ are present). Accordingly, the solution of the evolution equation (C4) takes the general form

$$\begin{aligned}
& U(x, s; \mu_F^2, \mu_0^2) \\
&= \sum_{n=0}^{\infty} ' E_n(\mu_F^2, \mu_0^2) \left[C_n^{3/2}(2x-1) + \frac{\alpha_s(\mu_F^2)}{4\pi} \sum_{k=n+2}^{\infty} ' d_{kn}^{(1)}(\mu_F^2, \mu_0^2) C_k^{3/2}(2x-1) + \mathcal{O}(\alpha_s^3) \right] \\
&\quad \times \frac{x(1-x)}{N_n} C_n^{3/2}(2s-1). \tag{C9}
\end{aligned}$$

The effect of the diagonal terms $\gamma_{nn} \equiv \gamma_n$ is completely contained in the factor $E_n(\mu_F^2, \mu_0^2)$, which is given by

$$E_n(\mu_F^2, \mu_0^2) = \exp \left[- \int_{\alpha_s(\mu_0^2)}^{\alpha_s(\mu_F^2)} d\alpha_s \frac{\gamma_n(\alpha_s)}{2\beta(\alpha_s)} \right]. \tag{C10}$$

The expansion of the anomalous dimensions in terms of α_s reads

$$\gamma_n(\alpha_s(\mu^2)) = \frac{\alpha_s(\mu^2)}{4\pi} \gamma_n^{(0)} + \frac{\alpha_s^2(\mu^2)}{(4\pi)^2} \gamma_n^{(1)} + \dots, \tag{C11a}$$

whereas the lowest order anomalous dimensions can be represented in closed form by

$$\gamma_n^{(0)} = 2C_F \left[4S_1(n+1) - 3 - \frac{2}{(n+1)(n+2)} \right] \tag{C11b}$$

with $S_1(n+1) = \sum_{i=1}^{n+1} 1/i = \psi(n+2) + \psi(1)$, while the function $\psi(z)$ is defined as $\psi(z) = d \ln \Gamma(z) / dz$. Since the anomalous dimensions γ_n coincide with the flavor non-singlet anomalous dimensions, i.e., the moments of the splitting kernels in deep inelastic scattering, we can use for $\gamma_n^{(1)}$ the results obtained in [131, 132]; viz.,

$$\gamma_0^{(1)} = 0, \quad \gamma_2^{(1)} = \frac{830}{81} N_f - \frac{34450}{243}, \quad \gamma_4^{(1)} = \frac{31132}{2025} N_f - \frac{662846}{3375}, \tag{C11c}$$

where N_f denotes the number of active flavors.¹² The nondiagonal matrix elements γ_{kn} ($k > n$) manifest themselves in the $d_{kn}^{(1)}$ terms of the eigenfunctions expansion and were obtained in closed form in [70, 71, 130]:

$$d_{kn}^{(1)}(\mu_F^2, \mu_0^2) = 2 \frac{N_n}{N_k} S_{kn}(\mu_F^2, \mu_0^2) C_{kn}^{(1)}, \tag{C12}$$

where

$$S_{kn}(\mu_F^2, \mu_0^2) = \frac{\gamma_k^{(0)} - \gamma_n^{(0)}}{\gamma_k^{(0)} - \gamma_n^{(0)} - 2b_0} \left\{ 1 - \left[\frac{\alpha_s(\mu_F^2)}{\alpha_s(\mu_0^2)} \right]^{-1 + (\gamma_k^{(0)} - \gamma_n^{(0)})/(2b_0)} \right\} \tag{C13a}$$

¹² For $Q^2 = 1.7 - 18.5 \text{ GeV}^2$ this number is 4, whereas for still higher Q^2 values, it starts to be equal 5.

and

$$C_{kn}^{(1)} = (2n+3) \left\{ \frac{-\gamma_n^{(0)} - 2b_0 + 8C_F A_{kn}}{2(k-n)(k+n+3)} + \frac{2C_F [A_{kn} - \psi(k+2) + \psi(1)]}{(n+1)(n+2)} \right\} \quad (\text{C13b})$$

with

$$A_{kn} = \psi\left(\frac{k+n+4}{2}\right) - \psi\left(\frac{k-n}{2}\right) + 2\psi(k-n) - \psi(k+2) - \psi(1). \quad (\text{C13c})$$

We turn now our attention to the finite-order solutions of the evolution equation (C4), i.e., (C1). Denoting the formal solution of the LO equation, which contains only the V_0 kernel, by $U^{\text{LO}}(x, s; \mu_F^2, \mu_0^2)$, the corresponding function E_n , defined in Eq. (C10), becomes

$$E_n^{\text{LO}}(\mu_F^2, \mu_0^2) = \left[\frac{\alpha_s(\mu_F^2)}{\alpha_s(\mu_0^2)} \right]^{\gamma_n^{(0)}/(2b_0)}. \quad (\text{C14})$$

Analogously, the solution of the NLO equation, containing both kernels V_0 and V_1 , will be represented by $U^{\text{NLO}}(x, s; \mu_F^2, \mu_0^2)$. This expression contains contributions coming from both the diagonal (E_n) and the nondiagonal ($d_{kn}^{(1)}$) parts. One finds in the literature two representations for the $E_n^{\text{NLO}}(\mu_F^2, \mu_0^2)$ function. The form which retains the manifest renormalization-group property $[E_n^{\text{NLO}}(\mu_1^2, \mu_2^2) E_n^{\text{NLO}}(\mu_2^2, \mu_3^2) = E_n^{\text{NLO}}(\mu_1^2, \mu_3^2)]$ reads [130]

$$E_n^{\text{NLO}}(\mu_F^2, \mu_0^2) = \frac{e_n(\mu_F^2)}{e_n(\mu_0^2)}; \quad \omega(n) \equiv \frac{\gamma_n^{(1)} b_0 - \gamma_n^{(0)} b_1}{2b_0 b_1}; \quad (\text{C15})$$

$$e_n(\mu_F^2) \equiv \left[\alpha_s(\mu_F^2) \right]^{\gamma_n^{(0)}/(2b_0)} \left[1 + \frac{b_1}{4\pi b_0} \alpha_s(\mu_F^2) \right]^{\omega(n)}. \quad (\text{C16})$$

Alternatively, one can recast E_n^{NLO} in the form [26, 133]

$$\widehat{E}_n^{\text{NLO}}(\mu_F^2, \mu_0^2) = \left[\frac{\alpha_s(\mu_F^2)}{\alpha_s(\mu_0^2)} \right]^{\gamma_n^{(0)}/(2b_0)} \left\{ 1 + \frac{b_1}{4\pi b_0} \alpha_s(\mu_F^2) \left[1 - \frac{\alpha_s(\mu_0^2)}{\alpha_s(\mu_F^2)} \right] \omega(n) \right\}, \quad (\text{C17})$$

which corresponds to a resummation of the leading logarithms associated with the diagonal terms, while the subleading ones are expanded with respect to α_s . In this work we employ (C15).¹³

Finally, we systematize below some previous results by recasting them in a form that is more suitable for practical purposes. As mentioned in previous sections, the coefficients $a_n(\mu_F^2)$ encapsulate nonperturbative information about the binding dynamics inside the pion and correspond to matrix elements of local operators according to the OPE, determined at some low-energy scale, characteristic of the nonperturbative dynamics employed [1, 91, 94, 134, 135]. To obtain these coefficients at a higher scale, say, μ_F^2 , one has to apply LO or

¹³ The expression (C15) is obtained by expanding γ_n and β to NLO in Eq. (C10) and integrating over α_s . To obtain the form (C17), one expands the integrand in (C10) over α_s and performs subsequently the integration.

NLO ERBL evolution. Specifically the coefficients which correspond to the LO evolution equation are given by

$$a_n^{\text{LO}}(\mu_F^2) = a_n^{\text{D,LO}}(\mu_F^2) = a_n(\mu_0^2) E_n^{\text{LO}}(\mu_F^2, \mu_0^2), \quad (\text{C18})$$

while those corresponding to the NLO evolution equation can be written in the form

$$a_n^{\text{NLO}}(\mu_F^2) = a_n^{\text{D,NLO}}(\mu_F^2) + \frac{\alpha_s(\mu_F^2)}{4\pi} a_n^{\text{ND,NLO}}(\mu_F^2), \quad (\text{C19a})$$

where

$$a_n^{\text{D,NLO}}(\mu_F^2) = a_n(\mu_0^2) E_n^{\text{NLO}}(\mu_F^2, \mu_0^2), \quad (\text{C19b})$$

$$a_n^{\text{ND,NLO}}(\mu_F^2) = \sum_{k=0}^{n-2} a_k(\mu_0^2) E_k^{\text{NLO}}(\mu_F^2, \mu_0^2) d_{nk}^{(1)}(\mu_F^2, \mu_0^2). \quad (\text{C19c})$$

We note that using instead of (C15) the expression (C17), would introduce only minor numerical corrections in the a_n^{NLO} coefficients of the order α_s^2 (amounting to, for example, a 1% relative deviation in a_n^{NLO} at 10 GeV²).

APPENDIX D: NLO EVOLUTION BY TAKING INTO ACCOUNT HEAVY-QUARK THRESHOLDS

We describe here the modification of the evolution formulas, presented in Appendix C, due to the inclusion of heavy-flavor thresholds at $M_4 = 1.3$ GeV and $M_5 = 4.3$ GeV (with $M_1 = M_2 = M_3 = 0$). First of all, for calculational convenience, we limit our study to pion DAs that include at the initial scale μ_0^2 only two Gegenbauer coefficients (i.e., eigenfunctions)

$$\varphi_\pi(x, \mu_0^2) = 6x(1-x) \left[1 + a_2^0 C_2^{3/2}(2x-1) + a_4^0 C_4^{3/2}(2x-1) \right] \quad (\text{D1})$$

and rewrite expressions (C19) in terms of these coefficients $\{a_2^0, a_4^0\}$ in the more compact form

$$a_2^{\text{NLO}}(\mu_F^2) = \tilde{E}_2(\mu_F^2, \mu_0^2) a_2^0 + \tilde{D}_{20}(\mu_F^2, \mu_0^2); \quad (\text{D2a})$$

$$a_4^{\text{NLO}}(\mu_F^2) = \tilde{E}_4(\mu_F^2, \mu_0^2) a_4^0 + \tilde{D}_{42}(\mu_F^2, \mu_0^2) a_2^0 + \tilde{D}_{40}(\mu_F^2, \mu_0^2); \quad (\text{D2b})$$

$$a_{n>4}^{\text{NLO}}(\mu_F^2) = \tilde{D}_{n4}(\mu_F^2, \mu_0^2) \tilde{E}_4(\mu_F^2, \mu_0^2) a_4^0 + \tilde{D}_{n2}(\mu_F^2, \mu_0^2) \tilde{E}_2(\mu_F^2, \mu_0^2) a_2^0 + \tilde{D}_{n0}(\mu_F^2, \mu_0^2), \quad (\text{D2c})$$

where

$$\tilde{D}_{nk}(\mu_F^2, \mu_0^2) \equiv \frac{\alpha_s(\mu_F^2)}{4\pi} d_{nk}^{(1)}(\mu_F^2, \mu_0^2). \quad (\text{D2d})$$

We start the evolution from the initial scale $\mu_0^2 = 1$ GeV², which corresponds to $N_f = 3$. When $\mu_F^2 \in [M_4^2, M_5^2]$, we need to change our evolution formulas by adopting the value $N_f = 4$. Finally, when $\mu_F^2 \geq M_5^2$, we need to use the value $N_f = 5$. Besides changing the number of active flavors N_f , we need also to match the initial conditions of evolution in

each considered region. This generates the following evolution functions (omitting in the following expressions the superscript NLO):

$$\tilde{E}_n(\mu_F^2, \mu_0^2) = \begin{cases} E_n(\mu_F^2, \mu_0^2; N_f = 3), & \mu_F^2 \leq M_4^2, \\ E_n(\mu_F^2, M_4^2; N_f = 4) \tilde{E}_n(M_4^2, \mu_0^2), & \mu_F^2 \in (M_4^2, M_5^2], \\ E_n(\mu_F^2, M_5^2; N_f = 5) \tilde{E}_n(M_5^2, \mu_0^2), & \mu_F^2 > M_5^2. \end{cases} \quad (\text{D3a})$$

We define in this way the diagonal part of the evolution equation from a fixed initial scale μ_0^2 using

$$\tilde{E}_n(\mu_F^2, q^2) \equiv \tilde{E}_n(\mu_F^2, \mu_0^2) \tilde{E}_n^{-1}(q^2, \mu_0^2). \quad (\text{D3b})$$

In this way we are able to derive the non-diagonal evolution functions (for the sake of brevity, we omit the explicit indication of the corresponding μ_F^2 regions); namely,

$$\tilde{D}_{20}(\mu_F^2, \mu_0^2) = \begin{cases} D_{20}(\mu_F^2, \mu_0^2; N_f = 3), \\ D_{20}(\mu_F^2, M_4^2; N_f = 4) + \tilde{E}_2(\mu_F^2, M_4^2) \tilde{D}_{20}(M_4^2, \mu_0^2), \\ D_{20}(\mu_F^2, M_5^2; N_f = 5) + \tilde{E}_2(\mu_F^2, M_5^2) \tilde{D}_{20}(M_5^2, \mu_0^2); \end{cases} \quad (\text{D4})$$

$$\tilde{D}_{40}(\mu_F^2, \mu_0^2) = \begin{cases} D_{40}(\mu_F^2, \mu_0^2; N_f = 3), \\ D_{40}(\mu_F^2, M_4^2; N_f = 4) + \tilde{E}_4(\mu_F^2, M_4^2) \tilde{D}_{40}(M_4^2, \mu_0^2), \\ D_{40}(\mu_F^2, M_5^2; N_f = 5) + \tilde{E}_4(\mu_F^2, M_5^2) \tilde{D}_{40}(M_5^2, \mu_0^2); \end{cases} \quad (\text{D5})$$

$$\tilde{D}_{42}(\mu_F^2, \mu_0^2) = \begin{cases} D_{42}(\mu_F^2, \mu_0^2; N_f = 3) \tilde{E}_2(\mu_F^2, \mu_0^2), \\ D_{42}(\mu_F^2, M_4^2; N_f = 4) \tilde{E}_2(\mu_F^2, \mu_0^2) + \tilde{E}_4(\mu_F^2, M_4^2) \tilde{D}_{42}(M_4^2, \mu_0^2), \\ D_{42}(\mu_F^2, M_5^2; N_f = 5) \tilde{E}_2(\mu_F^2, \mu_0^2) + \tilde{E}_4(\mu_F^2, M_5^2) \tilde{D}_{42}(M_5^2, \mu_0^2). \end{cases} \quad (\text{D6})$$

For $n > 4$ and $k = 0, 2, 4$, we have

$$\tilde{D}_{nk}(\mu_F^2, \mu_0^2) = \begin{cases} D_{nk}(\mu_F^2, \mu_0^2; N_f = 3), \\ \tilde{E}_n(\mu_F^2, M_4^2) \tilde{E}_k^{-1}(\mu_F^2, M_4^2) D_{nk}(\mu_F^2, M_4^2; N_f = 4) + \tilde{D}_{nk}(M_4^2, \mu_0^2), \\ \tilde{E}_n(\mu_F^2, M_5^2) \tilde{E}_k^{-1}(\mu_F^2, M_5^2) D_{nk}(\mu_F^2, M_5^2; N_f = 5) + \tilde{D}_{nk}(M_5^2, \mu_0^2). \end{cases} \quad (\text{D7})$$

Using these expressions, we can revert to our previous formulas (C19) and write

$$a_n^{\text{NLO}}(\mu_F^2) = a_n^{\text{D,NLO}}(\mu_F^2) + \frac{\alpha_s(\mu_F^2)}{4\pi} a_n^{\text{ND,NLO}}(\mu_F^2), \quad (\text{D8a})$$

where

$$a_n^{\text{D,NLO}}(\mu_F^2) = a_n(\mu_0^2) \tilde{E}_n(\mu_F^2, \mu_0^2), \quad (\text{D8b})$$

$$a_n^{\text{ND,NLO}}(\mu_F^2) = \sum_{k=0}^{n-2} a_k(\mu_0^2) \tilde{E}_k(\mu_F^2, \mu_0^2) \tilde{d}_{nk}^{(1)}(\mu_F^2, \mu_0^2) \quad (\text{D8c})$$

with

$$\tilde{d}_{nk}^{(1)}(\mu_F^2, \mu_0^2) \equiv \left[\frac{4\pi}{\alpha_s(\mu_F^2)} \right] \tilde{D}_{nk}(\mu_F^2, \mu_0^2). \quad (\text{D8d})$$

APPENDIX E: EVOLUTION OF THE PION DISTRIBUTION AMPLITUDE IN ANALYTIC PERTURBATION THEORY

The pion DA satisfies an evolution equation of the form

$$\frac{d\varphi_\pi(x, \mu_F^2)}{d \ln \mu_F^2} = V(x, u, \bar{\alpha}_s(\mu_F^2)) \otimes_u \varphi_\pi(u, \mu_F^2), \quad (\text{E1})$$

with $V(x, u, \alpha)$ having the same functional dependence on α as in (C2). Let us rewrite this equation for the coefficients of expansion (C5) in terms of Gegenbauer polynomials, using the notations proposed in [130] and linking them to those in [71]:

$$\begin{aligned} \frac{da_n(\mu_F^2)}{d \ln \mu_F^2} &= \frac{-\bar{\alpha}_s(\mu_F^2)}{8\pi} \left[\gamma_n^{(0)} + \frac{\bar{\alpha}_s(\mu_F^2)}{4\pi} \gamma_n^{(1)} \right] a_n(\mu_F^2) + \frac{1}{2} \left[\frac{\bar{\alpha}_s(\mu_F^2)}{4\pi} \right]^2 \sum_{0 \leq j < n} ' M_{j,n} a_j(\mu_F^2), \\ M_{j,n} &= 2 \frac{N_j}{N_n} C_{nj}^{(1)} [\gamma_n^{(0)} - \gamma_j^{(0)}]. \end{aligned} \quad (\text{E2})$$

First, we define the diagonal evolution operator $\hat{E}_n^{\text{NLO}}(Q^2, \mu_0^2) = \hat{e}_n(L_Q)/\hat{e}_n(L_{\mu_0})$ with

$$\frac{d\hat{e}_n(L_\mu)}{dL_\mu} = \frac{-\bar{\alpha}_s^{(2,\text{fit})}(\mu^2)}{8\pi} \left[\gamma_n^{(0)} + \frac{\bar{\alpha}_s^{(2,\text{fit})}(\mu^2)}{4\pi} \gamma_n^{(1)} \right] \hat{e}_n(L_\mu), \quad (\text{E3})$$

where $L_\mu \equiv \ln(\mu^2/\Lambda_{21}^2)$ and $\bar{\alpha}_s^{(2,\text{fit})}(\mu^2)$ is given by (6.22), i.e.,

$$\bar{\alpha}_s^{(2,\text{fit})}(\mu^2) = \frac{4\pi}{b_0(3)} \bar{a}_s[\ell(L_\mu, c_{21}^{\text{fit}})] \equiv \frac{4\pi}{b_0(3)} \bar{A}_s^{(2,\text{fit})}(L_\mu). \quad (\text{E4})$$

Then we have

$$\hat{e}_n^{\text{NLO}}(L_\mu) = \exp \left(- \int_{L_0}^{L_\mu} \left\{ \frac{\gamma_n^{(0)}}{2b_0(3)} \bar{A}_s^{(2,\text{fit})}(L) + \frac{\gamma_n^{(1)}}{2b_0(3)^2} [\bar{A}_s^{(2,\text{fit})}(L)]^2 \right\} dL \right). \quad (\text{E5})$$

In principle, the lower limit of integration, L_0 , can be chosen to be an arbitrary positive number, but it is more convenient to set it equal to the average value of $L[\mu_F^2]$ under actual consideration. Then, we can represent our solution in a modified form—as compared to (C19); namely,

$$a_n^{\text{An}}(\mu_F^2) = \hat{e}_n^{\text{NLO}}(L_{\mu_F}) \left[\frac{a_n(\mu_0^2)}{\hat{e}_n^{\text{NLO}}(L_{\mu_0})} + \frac{\bar{\alpha}_s(\mu_F^2)}{4\pi} \sum_{0 \leq j < n} ' \hat{d}_{j,n}(\mu_F^2, \mu_0^2) \frac{a_j(\mu_0^2)}{\hat{e}_j^{\text{NLO}}(L_{\mu_0})} \right]. \quad (\text{E6})$$

The advantage of introducing the same factor $\hat{e}_n^{\text{NLO}}[L_{\mu_F}]$ for the whole function $a_n^{\text{An}}(\mu_F^2)$ is that it ensures exact cancellation of the diagonal terms in Eq. (E2). What is left over after this cancellation provides an equation for $\hat{d}_{j,n}(\mu_F^2, \mu_0^2)$:

$$\begin{aligned} \frac{d \left[\bar{\alpha}_s(\mu_F^2) \hat{d}_{j,n}(\mu_F^2, \mu_0^2) \right]}{dL_{\mu_F}} &= \frac{\bar{\alpha}_s^2(\mu_F^2)}{8\pi} \left[M_{j,n} \frac{\hat{e}_j^{\text{NLO}}(L_{\mu_F})}{\hat{e}_n^{\text{NLO}}(L_{\mu_F})} \right. \\ &\quad \left. + \frac{\bar{\alpha}_s(\mu_F^2)}{4\pi} \sum_{j \leq m < n} ' \hat{d}_{j,m}(\mu_F^2, \mu_0^2) M_{m,n} \frac{\hat{e}_m^{\text{NLO}}(L_{\mu_F})}{\hat{e}_n^{\text{NLO}}(L_{\mu_F})} \right]. \end{aligned} \quad (\text{E7})$$

In the NLO approximation this expression becomes

$$\frac{d}{dL_{\mu_F}} \left[\bar{A}_s^{(2,\text{fit})}(L_{\mu_F}) \hat{d}_{j,n}(\mu_F^2, \mu_0^2) \right] \approx \frac{M_{j,n}}{2b_0(3)} \left[\bar{A}_s^{(2,\text{fit})}(L_{\mu_F}) \right]^2 \frac{\hat{e}_j^{\text{NLO}}(L_{\mu_F})}{\hat{e}_n^{\text{NLO}}(L_{\mu_F})} \quad (\text{E8})$$

and its solution is given by

$$\hat{d}_{j,n}(\mu_F^2, \mu_0^2) \approx \frac{M_{j,n}}{2b_0(3) \bar{A}_s^{(2,\text{fit})}(L_{\mu_F})} \int_{L_{\mu_0}}^{L_{\mu_F}} \left[\bar{A}_s^{(2,\text{fit})}(L) \right]^2 \frac{\hat{e}_j^{\text{NLO}}(L)}{\hat{e}_n^{\text{NLO}}(L)} dL. \quad (\text{E9})$$

Since we do not take into account the nondiagonal part of the evolution equation (see for more details in Sec. IV, just after Eq. (4.8)), we can use an approximate form of Eq. (E6), viz.,

$$a_n^{\text{An;D,NLO}}(\mu_F^2) = a_n(\mu_0^2) \frac{\hat{e}_n^{\text{NLO}}(L_{\mu_F})}{\hat{e}_n^{\text{NLO}}(L_{\mu_0})}, \quad (\text{E10})$$

where the functions $\hat{e}_n^{\text{NLO}}(L_{\mu_F})$ are defined in a two-step numerical procedure:

1. We determine first by numerical integration of Eq. (E5) the functions $\hat{e}_n^{\text{num}}(L)$ for $L \in [0, 10]$ and $n = 2, 4$.
2. We construct then interpolating functions $\hat{e}_n^{\text{NLO}}(L)$ for all functions determined in step one.

In order to obtain the term $\tilde{\mathcal{F}}_\pi^{\text{LO}}(\mu_F^2, \mu_R^2)$ in the approximate formula (4.15) for the factorized form factor, we also need the LO-part of the evolution, namely,

$$\hat{e}_n^{\text{LO}}(L_\mu) = \exp \left[- \int_{L_{\mu_0}}^{L_\mu} \frac{\gamma_n^{(0)}}{2b_0(3)} \bar{A}_s^{(2,\text{fit})}(L) dL \right]; \quad (\text{E11})$$

$$a_n^{\text{An;LO}}(\mu_F^2) = a_n(\mu_0^2) \frac{\hat{e}_n^{\text{LO}}(L_{\mu_F})}{\hat{e}_n^{\text{LO}}(L_{\mu_0})}. \quad (\text{E12})$$

-
- [1] A. P. Bakulev, S. V. Mikhailov, and N. G. Stefanis, Phys. Lett. **B508**, 279 (2001); *ibid.* **B590**, 309(E) (2004).
 - [2] I. L. Solovtsov and D. V. Shirkov, Theor. Math. Phys. **120**, 1220 (1999).
 - [3] D. V. Shirkov, Theor. Math. Phys. **127**, 409 (2001).
 - [4] D. V. Shirkov (2000), hep-ph/0003242.
 - [5] D. V. Shirkov, Theor. Math. Phys. **127**, 409 (2001).
 - [6] D. V. Shirkov, Eur. Phys. J. **C22**, 331 (2001).
 - [7] V. L. Chernyak and A. R. Zhitnitsky, JETP Lett. **25**, 510 (1977).
 - [8] V. L. Chernyak, A. R. Zhitnitsky, and V. G. Serbo, JETP Lett. **26**, 594 (1977).
 - [9] A. V. Efremov and A. V. Radyushkin, Phys. Lett. **B94**, 245 (1980).
 - [10] A. V. Efremov and A. V. Radyushkin, Theor. Math. Phys. **42**, 97 (1980).
 - [11] G. P. Lepage and S. J. Brodsky, Phys. Lett. **B87**, 359 (1979).
 - [12] G. P. Lepage and S. J. Brodsky, Phys. Rev. **D22**, 2157 (1980).

- [13] V. L. Chernyak and A. R. Zhitnitsky, Phys. Rept. **112**, 173 (1984).
- [14] S. J. Brodsky and G. P. Lepage, Adv. Ser. Direct. High Energy Phys. **5**, 93
- [15] A. H. Mueller, Nucl. Phys. **A622**, 3c (1997).
- [16] N. G. Stefanis, Eur. Phys. J. direct **C7**, 1 (1999).
- [17] K. Goeke, M. V. Polyakov, and M. Vanderhaeghen, Prog. Part. Nucl. Phys. **47**, 401 (2001).
- [18] N. Isgur and C. H. Llewellyn Smith, Phys. Rev. Lett. **52**, 1080 (1984).
- [19] O. C. Jacob and L. S. Kisslinger, Phys. Rev. Lett. **56**, 225 (1986).
- [20] N. Isgur and C. H. Llewellyn Smith, Nucl. Phys. **B317**, 526 (1989).
- [21] R. Jakob and P. Kroll, Phys. Lett. **B315**, 463 (1993); *ibid.* **B319**, 545(E) (1993).
- [22] M. A. Shifman, A. I. Vainshtein, and V. I. Zakharov, Nucl. Phys. **B147**, 385 (1979).
- [23] V. A. Nesterenko and A. V. Radyushkin, Phys. Lett. **B115**, 410 (1982).
- [24] A. V. Radyushkin, Acta Phys. Polon. **B26**, 2067 (1995).
- [25] A. P. Bakulev, A. V. Radyushkin, and N. G. Stefanis, Phys. Rev. **D62**, 113001 (2000).
- [26] B. Melić, B. Nžić, and K. Passek, Phys. Rev. **D60**, 074004 (1999).
- [27] B. Melić, B. Nžić, and K. Passek, Phys. Rev. **D65**, 053020 (2002).
- [28] N. G. Stefanis, W. Schroers, and H.-C. Kim, Phys. Lett. **B449**, 299 (1999).
- [29] N. G. Stefanis, W. Schroers, and H.-C. Kim, Eur. Phys. J. **C18**, 137 (2000).
- [30] B. Melić, D. Müller, and K. Passek-Kumerički, Phys. Rev. **D68**, 014013 (2003).
- [31] A. Khodjamirian, Eur. Phys. J. **C6**, 477 (1999).
- [32] V. M. Braun, A. Khodjamirian, and M. Maul, Phys. Rev. **D61**, 073004 (2000).
- [33] J. Bijnens and A. Khodjamirian, Eur. Phys. J. **C26**, 67 (2002).
- [34] A. P. Bakulev, S. V. Mikhailov, and N. G. Stefanis (2003), talk presented at the LC03 Workshop On Hadrons and Beyond, Durham, England, 5-9 Aug 2003, hep-ph/0310267.
- [35] J. Gronberg et al. (CLEO), Phys. Rev. **D57**, 33 (1998).
- [36] J. Volmer et al. (The Jefferson Lab F(π)), Phys. Rev. Lett. **86**, 1713 (2001).
- [37] H. P. Blok, G. M. Huber, and D. J. Mack (2002), nucl-ex/0208011.
- [38] A. Schmedding and O. Yakovlev, Phys. Rev. **D62**, 116002 (2000).
- [39] A. P. Bakulev, S. V. Mikhailov, and N. G. Stefanis, Phys. Rev. **D67**, 074012 (2003).
- [40] A. P. Bakulev, S. V. Mikhailov, and N. G. Stefanis, Phys. Lett. **B578**, 91 (2004).
- [41] A. V. Radyushkin and R. Ruskov, Nucl. Phys. **B481**, 625 (1996).
- [42] R. Jakob, P. Kroll, and M. Raulfs, J. Phys. **G22**, 45 (1996).
- [43] P. Kroll and M. Raulfs, Phys. Lett. **B387**, 848 (1996).
- [44] I. V. Musatov and A. V. Radyushkin, Phys. Rev. **D56**, 2713 (1997).
- [45] S. J. Brodsky, C.-R. Ji, A. Pang, and D. G. Robertson, Phys. Rev. **D57**, 245 (1998).
- [46] M. Diehl, P. Kroll, and C. Vogt, Eur. Phys. J. **C22**, 439 (2001).
- [47] A. P. Bakulev, S. V. Mikhailov, and N. G. Stefanis (2003), invited contribution to the Festschrift in honor of Prof. Anatoly Efremov's 70th birthday, hep-ph/0312141.
- [48] S. S. Agaev, Phys. Rev. **D69**, 094010 (2004).
- [49] T. Huang, X. G. Wu, and X. H. Wu (2004), hep-ph/0404163.
- [50] T. Gousset and B. Pire, Phys. Rev. **D51**, 15 (1995).
- [51] F. D. R. Bonnet, R. G. Edwards, G. T. Fleming, R. Lewis, and D. G. Richards (LHPC) (2003).
- [52] F. D. R. Bonnet, R. G. Edwards, G. T. Fleming, R. Lewis, and D. G. Richards (2003).
- [53] Y. Nemoto (RBC) (2003), hep-lat/0309173.
- [54] Y. L. Dokshitzer, G. Marchesini, and B. R. Webber, Nucl. Phys. **B469**, 93 (1996).
- [55] G. Grunberg (1997), hep-ph/9705290.

- [56] D. V. Shirkov and I. L. Solovtsov, Phys. Rev. Lett. **79**, 1209 (1997).
- [57] D. V. Shirkov, Theor. Math. Phys. **119**, 438 (1999).
- [58] E. Gardi, G. Grunberg, and M. Karliner, JHEP **07**, 007 (1998).
- [59] A. V. Nesterenko, Int. J. Mod. Phys. **A18**, 5475 (2003).
- [60] A. I. Karanikas and N. G. Stefanis, Phys. Lett. **B504**, 225 (2001).
- [61] N. G. Stefanis, Lect. Notes Phys. **616**, 153 (2003).
- [62] S. J. Brodsky, G. P. Lepage, and P. B. Mackenzie, Phys. Rev. **D28**, 228 (1983).
- [63] C.-R. Ji and F. Amiri, Phys. Rev. **D42**, 3764 (1990).
- [64] S. V. Mikhailov and A. V. Radyushkin, JETP Lett. **43**, 712 (1986).
- [65] S. V. Mikhailov and A. V. Radyushkin, Sov. J. Nucl. Phys. **49**, 494 (1989).
- [66] S. V. Mikhailov and A. V. Radyushkin, Phys. Rev. **D45**, 1754 (1992).
- [67] A. P. Bakulev and A. V. Radyushkin, Phys. Lett. **B271**, 223 (1991).
- [68] A. P. Bakulev and S. V. Mikhailov, Z. Phys. **C68**, 451 (1995).
- [69] N. G. Stefanis, Mod. Phys. Lett. **A10**, 1419 (1995).
- [70] D. Müller, Phys. Rev. **D49**, 2525 (1994).
- [71] D. Müller, Phys. Rev. **D51**, 3855 (1995).
- [72] V. M. Belyaev and B. L. Ioffe, Sov. Phys. JETP **57**, 716 (1983).
- [73] A. A. Ovchinnikov and A. A. Pivovarov, Sov. J. Nucl. Phys. **48**, 721 (1988).
- [74] A. L. Kataev, G. Parente, and A. V. Sidorov, Phys. Part. Nucl. **34**, 20 (2003).
- [75] M. D’Elia, A. Di Giacomo, and E. Meggiolaro, Phys. Rev. **D59**, 054503 (1999).
- [76] A. P. Bakulev and S. V. Mikhailov, Phys. Rev. **D65**, 114511 (2002).
- [77] B. Melić, B. Nizić, and K. Passek (2001), IRB-TH-02/01, hep-ph/0107311.
- [78] W. Celmaster and P. M. Stevenson, Phys. Lett. **B125**, 493 (1983).
- [79] V. Anisovich, D. Melikhov, and V. Nikonov, Phys. Rev. **D52**, 5295 (1995).
- [80] E. P. Kadantseva, S. V. Mikhailov, and A. V. Radyushkin, Sov. J. Nucl. Phys. **44**, 326 (1986).
- [81] R. D. Field, R. Gupta, S. Otto, and L. Chang, Nucl. Phys. **B186**, 429 (1981).
- [82] F. M. Dittes and A. V. Radyushkin, Sov. J. Nucl. Phys. **34**, 293 (1981).
- [83] M. H. Sarmadi, PhD dissertation, Pittsburgh University (1983), UMI 83-18195.
- [84] A. V. Radyushkin and R. S. Khalmuradov, Sov. J. Nucl. Phys. **42**, 289 (1985).
- [85] E. Braaten and S.-M. Tse, Phys. Rev. **D35**, 2255 (1987).
- [86] K. Hagiwara et al. (Particle Data Group), Phys. Rev. **D66**, 010001 (2002).
- [87] N. G. Stefanis, Nuovo Cim. **A83**, 205 (1984).
- [88] H.-n. Li and G. Sterman, Nucl. Phys. **B381**, 129 (1992).
- [89] A. V. Radyushkin, in *Perspectives in Hadronic Physics: Proceedings of the ICTP Conference, 12-16 May 1997, Trieste, Italy*, edited by S. Boffi, C. C. D. Atti, and M. Giannini (World Scientific, Singapore, 1997), pp. 126–135.
- [90] H. J. Behrend et al. (CELLO), Z. Phys. **C49**, 401 (1991).
- [91] V. Y. Petrov, M. V. Polyakov, R. Ruskov, C. Weiss, and K. Goeke, Phys. Rev. **D59**, 114018 (1999).
- [92] M. Praszalowicz and A. Rostworowski, Phys. Rev. **D64**, 074003 (2001).
- [93] S. Dalley and B. van de Sande (2002), hep-ph/0212086.
- [94] I. V. Anikin, A. E. Dorokhov, and L. Tomio, Phys. Part. Nucl. **31**, 509 (2000).
- [95] B. A. Magradze, in *Proceedings of the 10th International Seminar Quarks’98, Suzdal, Russia, 18–24 May 1998*, edited by F. L. Bezrukov, V. A. Matveev, V. A. Rubakov, A. N. Tavkhelidze, and S. V. Troitsky (INR RAS, Moscow, 1999), pp. 158–171.
- [96] D. V. Shirkov and S. V. Mikhailov, Z. Phys. **C63**, 463 (1994).

- [97] G. Grunberg, Phys. Lett. **B95**, 70 (1980).
- [98] G. Grunberg, Phys. Rev. **D29**, 2315 (1984).
- [99] P. M. Stevenson, Phys. Lett. **B100**, 61 (1981).
- [100] P. M. Stevenson, Phys. Rev. **D23**, 2916 (1981).
- [101] P. Stevenson, Nucl. Phys. **B203**, 472 (1982).
- [102] P. M. Stevenson, Nucl. Phys. **B231**, 65 (1984).
- [103] V. M. Braun, G. P. Korchemsky, and D. Müller, Prog. Part. Nucl. Phys. **51**, 311 (2003).
- [104] G. P. Korchemsky, Phys. Lett. **B217**, 330 (1989).
- [105] G. P. Korchemsky, Phys. Lett. **B220**, 629 (1989).
- [106] G. C. Gellas, A. I. Karanikas, C. N. Ktorides, and N. G. Stefanis, Phys. Lett. **B412**, 95 (1997).
- [107] N. G. Stefanis (1998), hep-ph/9811262.
- [108] S. J. Brodsky and H. J. Lu, Phys. Rev. **D51**, 3652 (1995).
- [109] I. L. Solovtsov and D. V. Shirkov, Phys. Lett. **B442**, 344 (1998).
- [110] D. V. Shirkov and I. L. Solovtsov, Phys. Part. Nucl. **32S1**, 48 (2001).
- [111] A. V. Radyushkin, JINR Rapid Commun. **78**, 96 (1996), hep-ph/9907228.
- [112] N. V. Krasnikov and A. A. Pivovarov, Phys. Lett. **B116**, 168 (1982).
- [113] D. S. Kourashev and B. A. Magradze (2001), hep-ph/0104142.
- [114] D. S. Kurashev and B. A. Magradze, Theor. Math. Phys. **135**, 531 (2003).
- [115] V. A. Nesterenko and A. V. Radyushkin, Phys. Lett. **B128**, 439 (1983).
- [116] A. V. Radyushkin, Nucl. Phys. **A527**, 153C (1991).
- [117] A. P. Bakulev (1995), unpublished.
- [118] V. V. Braguta and A. I. Onishchenko (2004), hep-ph/0403240.
- [119] S. J. Brodsky, T. Huang, and G. P. Lepage, in *Particles and fields – 2: Proceedings of the Banff Summer Institute on Particles and Fields, Banff, Canada, Aug 16-27, 1981*, edited by A. Z. Capri and A. N. Kamal (Plenum Press, 1983), pp. 143–199.
- [120] L. S. Kisslinger and S. W. Wang, Nucl. Phys. **B399**, 63 (1993).
- [121] K. G. Chetyrkin, A. L. Kataev, and F. V. Tkachov, Phys. Lett. **B85**, 277 (1979).
- [122] C. N. Brown et al., Phys. Rev. **D8**, 92 (1973).
- [123] C. J. Bebek et al., Phys. Rev. **D13**, 25 (1976).
- [124] S. J. Brodsky and G. P. Lepage (1980), Invited talk given at 20th Int. Conf. on High Energy Physics, Madison, Wisc., Jul 17-23, 1980.
- [125] K. Passek, PhD dissertation, University of Zagreb (2001).
- [126] F. M. Dittes and A. V. Radyushkin, Phys. Lett. **B134**, 359 (1984).
- [127] M. H. Sarmadi, Phys. Lett. **B143**, 471 (1984).
- [128] S. V. Mikhailov and A. V. Radyushkin, Nucl. Phys. **B254**, 89 (1985).
- [129] G. R. Katz, Phys. Rev. **D31**, 652 (1985).
- [130] S. V. Mikhailov and A. V. Radyushkin, Nucl. Phys. **B273**, 297 (1986).
- [131] E. G. Floratos, D. A. Ross, and C. T. Sachrajda, Nucl. Phys. **B129**, 66 (1977).
- [132] A. Gonzalez-Arroyo, C. Lopez, and F. J. Yndurain, Nucl. Phys. **B153**, 161 (1979).
- [133] D. Müller, Phys. Rev. **D59**, 116003 (1999).
- [134] M. Praszalowicz and A. Rostworowski, Phys. Rev. **D64**, 074003 (2001).
- [135] A. E. Dorokhov, JETP Lett. **77**, 63 (2003).